Technical Report Documentation Page

1. Report No. FIU-EDPSE-04	2. Government Accession No.	3. Recipient's Catalog No.	
4. Title and Subtitle **Epoxy Dowel Pile Splice Evaluation**		5. Report Date March 2021 6. Performing Organization Code	
7. Author(s) Armin Mehrabi https://orcid.org/0000-0003-4736-850X Saman Farhangdoust https://orcid.org/0000-0002-5061-3513		8. Performing Organization Report No.	
9. Performing Organization Name and Address Department of Civil and Environmental Engineering Florida International University 10555 West Flagler Street, EC 3680 Miami, FL 33174		10. Work Unit No. (TRAIS) 11. Contract or Grant No. BDV29-977-52	
12. Sponsoring Organization Name and Address FDOT Research Center Phone: (850) 414-5260 605 Suwannee Street Tallahassee, Florida 32399-0450 Email: research.center@dot.state.fl.us		13. Type of Report and Period Covered Interim Report- Task 4 Deliverable 14. Sponsoring Agency Code	
15. Supplementary Notes			
16. Abstract For various reasons including limitations in shipping and operation as well as unforeseen soil conditions, it often happens that splicing of precast-prestressed concrete pile (PPCP) segments has to be performed at the site to achieve longer lengths. Epoxy dowel splices are commonly used in Florida. The objective of this study is to investigate the effectiveness of glass fiber reinforced polymer (GFRP) dowel bars proposed as an economic corrosion-resistant option for use in piles splices. The study is expected to develop design procedure and details for GFRP epoxy dowel splices, aims at recommending refinements to current designs, and develop design drawings for the recommended details. It will also develop an analytical framework that can be used for design of future variations of pile and splice systems. The primary focus will be on the flexural behavior of the pile splices. To date, an analysis procedure for design of splice using GFRP dowels has been developed, a series of test specimens using various combinations of dowel and strand types have been designed, constructed, and tested. This report covers Task 4 of the project and focuses on fabrication and laboratory test of 10 full-scale epoxy dowel splices using steel and corrosion resistance GFRP and CFRP as strands and dowels. The pile splices were developed for both drivable unforeseen and preplanned cases.			
17. Key Words Prestressed Precast Concrete Pile, Pile Splice, Epoxy Dowel Splice, CFRP, HSSS, SS, GFRP, bending test.		18. Distribution Statement No Restriction	
19. Security Classification Unclassified	20. Security Classification (of this page) Unclassified	21. No. of Pages 68	22. Price

(this page is intentionally left blank)

Epoxy Dowel Pile Splice Evaluation

Project No. BDV29-977-52

Interim Report – Task 4 Deliverable

Revised May 2021

Principal Investigator: Armin Mehrabi
Co-PI: David Garber
Co-PI: Seung Jae Lee
Graduate Assistant: Saman Farhangdoust

Department of Civil and Environmental Engineering
Florida International University
Miami, FL

Authors

Saman Farhangdoust
Armin Mehrabi

Sponsored by

FDOT
Florida Department of Transportation

A report from

FIU FLORIDA INTERNATIONAL UNIVERSITY

Contents

List of Figures

List of Tables

1 INTRODUCTION

This research intends to provide a better understanding of the performance and behavior of spliced bearing piles, along with a refined design that will be incorporated within the Florida Department of Transportation (FDOT) Standard Plans (Index 455-series). The objective of this project is to experimentally and analytically investigate the behavior and effectiveness of epoxy dowel splice for prestressed precast concrete piles using corrosion resistant material for the dowels, and comparing their performance to conventional carbon steel dowel splices. The primary focus is on the flexural behavior of the pile splices. This research project aims also to verify the GFRP dowels as a more economical alternative to other materials. The research is expected to develop design procedure and details for GFRP epoxy dowel splices, and if applicable, introduce refinements to the current designs for CFRP, stainless steel, and steel dowels, and develop design drawings for the recommended details. It will also develop an analytical framework that can be used in future for systems not covered in this project. Task 1 included a literature review that was completed in July 2019, and the report was submitted to FDOT. The second report was completed and submitted to FDOT in January 2020, which covers Task 2: Design calculations for the GFRP Epoxy Dowel Pile Splice capacities, and detailed drawings depicting the design for incorporation into the testing phase. The report of Task 3 was completed and submitted in December 2020. Detailed design and construction drawings of the test specimens, detailed drawings depicting the design for loading and instrumentation to monitor and record the flexural response of each splice configuration, and detailed calculations predicting the capacity of each pile splice test specimen were covered in Task 3. In Task 4 of this project that is the subject of this report, pile segments were fabricated and spliced at S&S Precast, Inc., an approved precast plant by FDOT, and were tested at the FDOT Structures Laboratory. This report covers the details of the fabrication and laboratory tests that were performed based on test matrix, instrumentation plans, test set up and procedures developed in Task 3 with some modifications as per the limitations of the precast plant.

2 FABRICATION

The fabrication and laboratory test of epoxy dowel splices were developed for 10 precast prestressed concrete pile specimens for both drivable unforeseen and preplanned pile splices. Each test specimen was comprised of two segments (14ft + 14ft), with a total length of 28 ft. The testing is limited to piles of 18x18 in. cross-section and focuses on the flexural resistance of pile splices.

2.1 Test Matrix

The original test matrix included the use of CFRP, SS, and GFRP dowel splices, as well as carbon steel dowels connecting pile segments of compatible material. As part of the investigation in Task 2, it became clear that the behavior of piles and splices using stainless steel (SS) material is expected to be similar to those using carbon steel material for strands and dowels. Accordingly, in coordination with the FDOT Project Manager (PM) and technical committee, the test matrix was modified by eliminating specimens using stainless steel material and adding to the number of specimens using GFRP dowels in combination with piles using CFRP and carbon steel strands. Additional changes were applied because of constructability and precast plant operation limitations. Because of availability issues, the precast plant requested to use Concrete Class V with nominal compressive strength of 6,500 psi instead of project specified Class V (Special) with compressive strength of 6,000 psi. The change was approved by FDOT PM. For ease of operation, the precast plant also asked to change the number and size of the steel strands in the pile segments from 16~0.5” to 12~0.6”. This was to have the same number and arrangement of strands for steel and CFRP strands so that they could be fabricated in the same casting bed. This request was evaluated by the research team and was approved. Accordingly, FIU team changed from 6’9” to 8’3” the strand development length and the dowel embedment length in the upper segment and for the auxiliary bar length in the lower segment. Also, as a consequence, the specified jacking force of the individual strands for the piles using CFRP strands was increased from the specified 34 kips to 35 kips to be consistent with the current design of FDOT Standard Plans for the steel strand of 0.6” diameter. It is believed these changes will not affect negatively the purpose of this study, since the main purpose of the study is to investigate the behavior at the splice region and performance of the dowels. In addition, in consultation with Tokyo Rope USA (TRUSA)and communication with the FDOT Project Manager (PM) and technical committee, the (9) #6 CFRP dowel was changed to (9) 7-strand 19.3 mm diameter CFRP for the test specimens 9 and 10. These dowels

have been reportedly used for splices in other investigations and have performed satisfactorily. The shop drawings prepared by S&S Precast containing all changes applied are shown in Appendix A. The updated test matrix shown in Table 1 was used for fabrication and flexural testing.

Table 1: Matrix of the test specimens

Dowel	Specimen	Pile 18x18" Strand	Splice for Drivable Unforeseen/Preplanned	Segment 1 Length-ft	Segment 2 Length-ft	Spliced Length-ft
GFRP	1	Steel SP-Index-455-018	Unforeseen SP-455 [See Shop Drawings in App. A]	14	14	28
	2	CFRP SP-Index 455-118	Unforeseen SP-455 [See Shop Drawings in App. A]	14	14	28
GFRP	3	Steel SP-Index-455-018	Preplanned SP-455 [See Shop Drawings in App. A]	14	14	28
	4	Steel SP-Index-455-018	Preplanned SP-455 [See Shop Drawings in App. A]	14	14	28
	5	CFRP SP-Index 455-118	Preplanned SP-455 [See Shop Drawings in App. A]	14	14	28
	6	CFRP SP-Index 455-118	Preplanned SP-455 [See Shop Drawings in App. A]	14	14	28
Steel	7	Steel SP-Index-455-018	Preplanned SP-455-002 [See Shop Drawings in App. A]	14	14	28
	8	Steel SP-Index-455-018	Preplanned SP-455-002 [See Shop Drawings in App. A]	14	14	28
CFRP	9	CFRP SP-Index 455-118	Preplanned SP-455-102 [See Shop Drawings in App. A]	14	14	28
	10	CFRP SP-Index 455-118	Preplanned SP-455-102 [See Shop Drawings in App. A]	14	14	28

2.2 Specimen Fabrication

Fabrication of the test specimens followed all relevant specifications within FDOT Standard Specifications [2020], especially in the notes and specifications within FDOT Standard Drawings

Index 455 with the exceptions noted above. The fabrication of the test specimens followed the shop drawings presented in Appendix A.

2.2.1 Forms and Preparations

Figure 1 shows the precast bed used for fabrication of the specimens. Wooden headers were used, along with a casting bed to construct the test specimens. Twelve holes were drilled in the headers to accommodate the CFRP and steel strands. According to the dowel arrangements, eight or nine holes were also drilled in the headers to accommodate the steel, CFRP, and GFRP dowels. In addition, spacing between wooden headers were used to allow for the embedment length required for the dowels of the "male" pile specimens (Figure 1, right photo).

Figure 1: Wooden headers arrangement in casting bed

As shown in Figure 2, the strands were delivered in spools. The strands were pulled from the spool along with the casting bed, while being fed through the headers. #10 steel dowels and strands were used for pile splices in accordance with the FDOT Standard Drawings Index 455-002 and 455-018.

Figure 2: Stand installation

Material properties of FRP dowel bars were expected to comply at minimum with the FDOT Specifications as shown in Table 2 below. Because of availability, the actual material used for FRP dowels varied from those in this table.

Table 2: Sizes and mechanical properties of FRP bars

Bar Size Designation	Nominal Bar Diameter (in)	Nominal Cross Sectional Area (in^2)	Measured Cross-Sectional Area (in^2)		Minimum Guaranteed Tensile Load (kips)	
			Minimum	Maximum	GFRP Bars	CFRP Bars
2	0.250	0.049	0.046	0.085	6.1	10.3
3	0.375	0.11	0.104	0.161	13.2	20.9
4	0.500	0.20	0.185	0.263	21.6	33.3
5	0.625	0.31	0.288	0.388	29.1	49.1
6	0.750	0.44	0.415	0.539	40.9	70.7
7	0.875	0.60	0.565	0.713	54.1	-
8	1.000	0.79	0.738	0.913	66.8	-
9	1.128	1.00	0.934	1.137	82.0	-
10	1.270	1.27	1.154	1.385	98.2	-

The exact material for the GFRP dowels were selected by the precast contractor (S&S Precast, Inc.) based on availability from V-Rod Material supplied by Pultral of Canada and communicated with the FDOT Project Manager to meet the requirements of ASTM D7957-17 and FDOT Standard Specification for Road and Bridge Construction [January 2020] Section 932.

According to proposed Drawings in Task 3 of this research, GFRP #10 and #8 bars were used as dowel and auxiliary bars, respectively (Figure 3) in accordance with the original design presented in Task 3 of this project.

Figure 3: The GFRP bars used for the construction

The modulus of elasticity and tensile strength of the GFRP bars reported by the supplier is included in the Table 3 (see Appendix B).

Table 3: The mechanical properties of the GFRP bars

Bar Size Designation	Minimum Tensile Module	Guaranteed Tensile Strength
8	7252 ksi	130.5 ksi
10	7252 ksi	116 ksi

The exact material for the CFRP strands and spirals were selected in consultation with TRUSA and communication with the FDOT project manager to meet the requirements of FDOT Standard Specification Section 933 (Figure 4). As stated earlier, the 7-strand 19.3mm ϕ strand material was

used instead of #6 CFRP bar for dowels. The modulus of elasticity and guaranteed breaking load of the 7-strand 19.3mm ϕ strand are 21,756 ksi and 106.9kips, respectively (see Appendix B)

Figure 4: The CFRP strands and spirals used for the construction

According to FDOT Standard Drawings Index 455, the holes for the "female" pile specimens were cast using 2-inch galvanized pipes for the preplanned Specimens 3-8, and 1 ½-inch galvanized pipes for Specimens 9 and 10 (Figure 5) meeting the requirements of ASTM A653, Coating Designation G90, 26 gauge. The holes for "Unforeseen Splice" specimens (Specimens 1 and 2) were to be drilled with 1 ¾ in. drill size. However, the contractor used 1 ¼-inch PVC pipes to first cast the holes, and then drilled 1 ¾-inch holes in the pipes to simulate field conditions.

Figure 5: The pipes used for the construction

As shown in Figure 6 (left), in accordance with Index 455-102, Note 4. “1” spiral tie pitch was considered to be continued to 4 ft below the head of the pile where the dowel holes are utilized. One full turn spiral was used to splice the spiral ties. Each wrap of the spiral strand was tied to a minimum of two corner strands. All CFRP and steel spirals were tied in their final position to strands with steel ties (Figure 6, upper right photo). According to the proposed drawings in Task 3 of this research, all auxiliary bars were installed with a distance of 1-inch from the chamfer (Figure 6, lower right photo).

Figure 6: The spirals, strands and bars configuration

2.2.2 Stressing

For this fabrication, all specimens were constructed, along with the same casting bed. Accordingly, to splice the CFRP strands to steel strands, the TRUSA couplers were used following strict

installation procedure prescribed by TRUSA (Figure 7). TRUSA engineer was present to train the precaster and inspect the procedure.

Figure 7: Coupling arrangement and installation by TRUSA

Figure 8 shows one of these special couplers in which the CFRP strand end installed with wedges and buffer materials was coupled to the steel strand end by twisting together the threaded ends of the sleeve and the coupler.

Figure 8: The steel strands (left) coupled with the CFRP stands (right)

As it was noted before, because of casting pile segments with steel and CFRP strands in the same bed, it was decided to apply the same tension force to each strand that is 35 kips. The calculated elongation corresponding to this tension force for CFRP and steel strands are shown in Table 4.

Table 4: Calculated elongations for steel and CFRP strands

Strand	Calculated Elongation		
	-5%	Target	+5%
CFRP elongation (in)	19.79	20.83	21.87
Steel elongation (in)	15.79	16.63	17.46
Total Elongation (in)	35.58	37.46	39.33

Table 4 shows the parameters used for calculation of total elongation for the CFRP strand based on TRUSA recommendations. The total elongation includes also an estimate of the wedges displacement in the CFRP anchoring device.

Table 5: Calculations for CFRP strand elongation

Symbol	Value	Unit	Description
ΔL_{CF}	19.020	in	Elongation of a CFRP
D_{WCF}	0.906	in	Insert displacement of the wedge into the sleeve while loading pre-stressing load
L_{CF}	283.000	ft	Length of CFRP
P	35.000	kips	Prestressing load
A_{CF}	0.217	sqin	Nominal effective area of CFRP
E_{CF}	2.88E+07	psi	Elastic modulus of CFRP
ΔL_{T-CF}	20.83	in	Total elongation of CFRP

The strand tensioning schedule/order is shown in Figure 9.

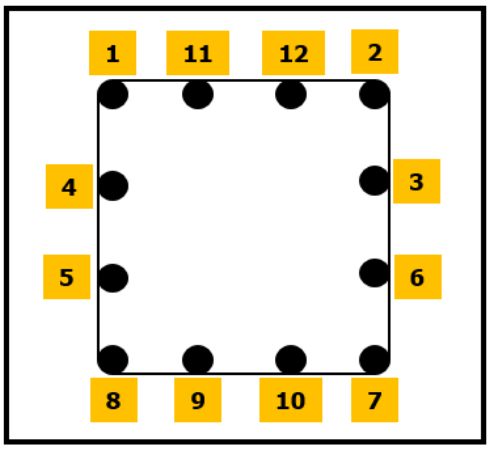

Figure 9: The stressing schedule

2.2.3 Concrete Casting

To cast all 10 piles, three truckloads of concrete were used. The top surface of the concrete was leveled to a smooth finish (Figure 10). Furthermore, cylindrical samples were collected during the

construction for future testing to determine the compressive strength of the concrete used for fabrication of the test specimens. Concrete pour for all specimens was carried out between 12:30 and 2pm on Friday, November 6, 2020. Temperature at the time of casting was in the range of 82°F to 88°F.

Figure 10: Casting concrete

2.2.4 Curing

The pile specimens were cured in the open field under ambient condition. The cylindrical samples to be used for compressive strength tests were moist cured per AASHTO R18 and ASTM C-31 specifications.

2.2.5 Cutting Strands- Strand Release

The strands were detensioned prior to removal of the forms and after the concrete cylinder tests indicated reaching the strength required for strand release per approved specifications. Detensioning was performed on Tuesday, November 10, 2020. The strand detensioning was performed per FDOT 450-11.3 by using a low-oxygen flame in accordance with a pattern/order provided in Figure 11. The side forms were removed after strand detensioning on the same day.

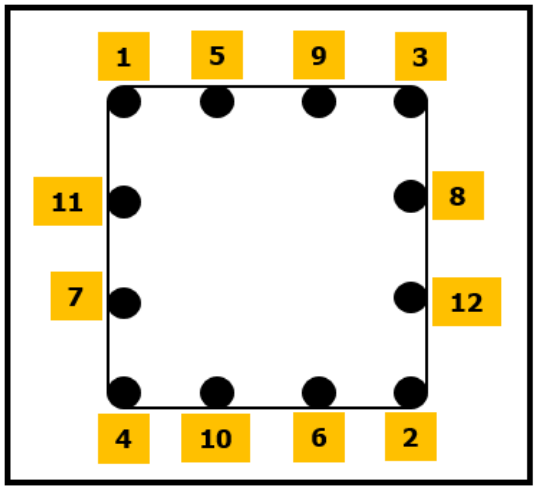

Figure 11: The detensioning schedule

Pile specimens were taken out from the casting bed on Tuesday (November 10, 2020) to be spliced after their concrete reached a minimum compressive strength of 80 percent of the nominal 28-day compressive strength.

3 SPLICING

A total of 20- 14-ft-long prestressed precast pile segments with a 18x18 in. cross-section were built at the S&S Precast, Inc. yard to be spliced based on the test matrix shown in Table 1. Figure 12 shows some of the prestressed precast pile segments.

Figure 12: Pile specimens using steel (left), GFRP (middle), and CFRP (right) dowels

3.1 Preparation

For the test specimens, holes are either cast or drilled into one end of the female pile segments to receive dowel rebars protruding out of the male pile segment. Specifically, for the "Unforeseen

Splice" specimens (Specimens 1 and 2), the holes were cast with 1 ¼-inch PVC pipes, and then 1 ¾-inch holes were drilled to simulate field conditions (Figure 13).

Figure 13: Drilling (left) and cleaning (right) the holes for Unforseen Splice specimens

Before installation, concrete members receiving dowels were checked to be structurally sound and free of cracks in the vicinity of the holes. The interior surfaces of the holes were cleaned to be free of loose particles, oil, and other contaminants (Figure 14). For installation, all debris, oils, and any other deleterious material from dowels were first removed to avoid contamination of the adhesive bonding material. As shown in Figure 14, the pile segments were assembled in a vertical alignment to mimic the site condition. The precast contractor (S&S Precast, Inc.), established a setup to first keep the 10 female pile specimens in a vertical position. The male pile segments were then installed with the use of crane one by one. A proper lifting device and suitable locations were determined to keep the segments balanced at the splice location.

Figure 14: Splice setup

To adequately fill the holes and cover the dowels with epoxy, a wooden framework was installed at the pile splice location before splicing (Figure 15).

Figure 15: Wooden framework used for splicing the pile specimens

3.2 Epoxy

In accordance with FDOT Standard Specification Sections 926 [2020], epoxy was used to fill the interface and sockets of the lower segment (female pile) so that the dowel bars of the upper segment (male pile) could be fully enveloped with the epoxy. Type AB Epoxy- Pilgrim EM 5-2 compound was used to fill the holes and form the joint between pile sections. The final mixture of this epoxy contained the A (epoxy) + B (curing agent) and C (aggregate). As shown in Figure 16, the kiln-dried 20-30 grade silica was used as the aggregate with the epoxy to increase its strength and reduce the potential shrinkage. In addition, some epoxy samples were collected for bond testing with concrete.

Figure 16: Epoxy mixture and sampling

The exact proportion of mixing sand with the epoxy and mixing process were determined in consultation with the FDOT project manager, the precast contractor (S&S Precast, Inc.) and the supplier (Pilgrim). Table 6 shows the details of the epoxy mixture used for the pile splicing. Two recommended ratios were used to make the final mixture by 1.5 to 1 volumes of silica to 1 volume of mixed epoxy. Because of the lower than expected temperature at the time of mixing (ranging from 61 to 77 F), the originally prescribed 1.5:1 (sand: epoxy) ratio resulted in low flowability. Therefore, it was decided to switch to 1:1 proportion. For splicing the pile specimens, different epoxy volumes were used for splicing based on the type of dowels.

Table 6: The ratio and volume of used Epoxy for the pile splicing

Pile Specimen Number	Mixture Ratio		Volume for one Round		Number of Rounds
	Epoxy	Sand	Epoxy	Sand	
1	1	1	2 gallons	2 gallons	~ 3
2	1	1	2 gallons	2 gallons	~ 3
3	1	1	2 gallons	2 gallons	~ 3
4	1	1	2 gallons	2 gallons	~ 3
5	1	1	2 gallons	2 gallons	~ 3
6	1	1.5	2 gallons	3 gallons	~ 3
7	1	1.5	2 gallons	3 gallons	~ 2
8	1	1	2 gallons	2 gallons	~ 2
9	1	1	2 gallons	2 gallons	~ 4
10	1	1	2 gallons	2 gallons	~ 4

3.3 Splicing

Piles were spliced with particular attention to the requirements and limitations due to ambient temperature and curing. As shown in Figure 17, adequate quantities of the epoxy were used to fill the drilled hole and the joint between segments at the splice to ensure no air voids. Table 7 shows the details and conditions of the pile splicing for all specimens.

Figure 17: Filling the holes by epoxy and assembling pile specimens

Table 7: Detailed conditions at splicing time

Specimen Number	Splicing Date	Weather Conditions	Moving date	Weather Conditions	Days Curing	Dunnage type
1	Tue, Dec. 15, 2020	75°, wind 4.9 mph W, overcast	Sat, Dec 19,02020	75°, wind 7.5 mph ESE, sunny	4	wood, 4 points
2	Mon, Dec. 14, 2020	77°, wind 9.3 mph SSW, cloudy	Sat, Dec 19,02020	75°, wind 7.5 mph ESE, sunny	5	wood, 4 points
3	Tue, Dec. 8, 2020	61°, wind 11.8 mph NW, sunny	Wed, Dec. 16, 2020	81°, wind 10.5 mph S, sunny	8	wood, 4 points
4	Thu, Dec. 10, 2020	72°, wind 4.9 mph N, sunny	Sat, Dec 19,02020	75°, wind 7.5 mph ESE, sunny	9	wood, 4 points
5	Wed, Dec. 9, 2020	64°, wind 4.9 mph N, sunny	Fri, Dec 18, 2020	68°, wind 10.5 mph NE, clear	9	wood, 4 points
6	Wed, Dec. 2, 2020	70°, wind 11.8 mph NE, sunny	Wed, Dec. 16, 2020	81°, wind 10.5 mph S, sunny	14	wood, 4 points
7	Tue, Dec. 1, 2020	66°, wind 8.0 mph N, cloudy	Wed, Dec. 16, 2020	81°, wind 10.5 mph S, sunny	15	wood, 4 points
8	Sat, Dec. 12, 2020	79°, wind 6.2 mph SW, cloudy	Fri, Dec 18, 2020	68°, wind 10.5 mph NE, clear	6	wood, 4 points
9	Fri, Dec. 11, 2020	73°, wind 9.30 mph ENE, sunny	Sat, Dec 19,02020	75°, wind 7.5 mph ESE, sunny	8	wood, 4 points
10	Fri, Dec. 4, 2020	77°, wind 9.3 mph SE, sunny	Wed, Dec 16, 2020	81°, wind 10.5 mph S, sunny	12	wood, 4 points

3.4 Storage and Shipping

The piles, once spliced, were left standing for a minimum of seven days for the epoxy to be fully cured, and then all spliced piles were lowered and placed on multiple supports, with two near the ends and two straddling the splice section in close proximity (Figure 18). The contractor used bridles, slings and other required handling equipment for supporting the splices during storage and shipment.

Figure 18: The spliced specimens

Nine cylindrical specimens for each batch of concrete were collected to determine the compressive strength at the time of flexural testing. The cylinders were tested at 28 days, and at the time of splice flexural testing. Cube samples of epoxy compound were also prepared and shipped to the laboratory for testing. Moreover, five 6-ft bars for each size and type of bars (steel and GFRP), as well as strand pieces for each size and type (steel and CFRP), were collected for tension testing.

4 EXPERIMENTAL PROGRAM

As shown in Figure 19, the assembled test specimens were installed in the test setup with extreme caution to avoid damage to the splice section. This testing program focused on the global behavior and flexural capacity of the epoxy dowel splices. The test specimens were instrumented to capture the flexural behavior of the splice.

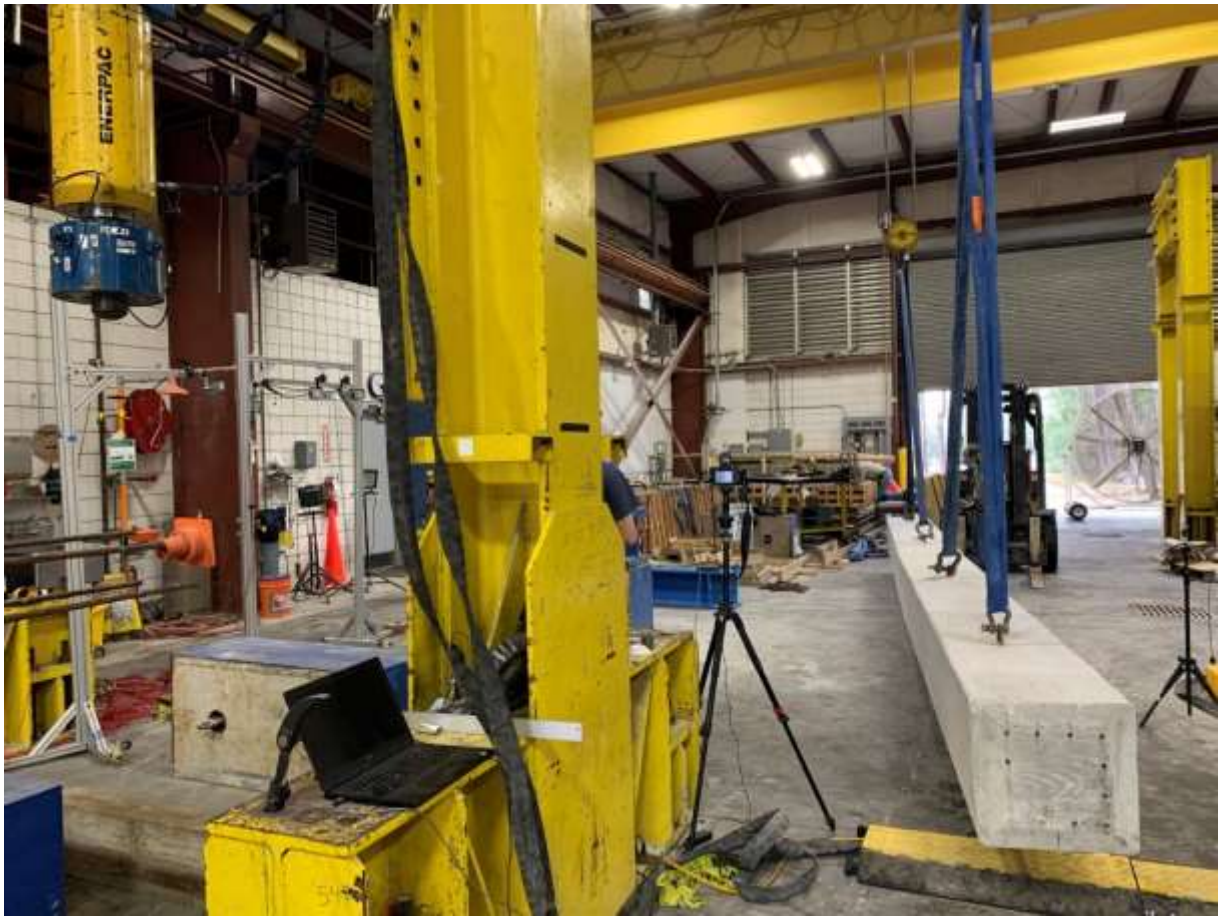

Figure 19: Test specimen installation

4.1 Instrumentation

Figures 20 and 21 show the schematic of the test setup and instrumentation from different views. The spliced specimens with a length of 28-ft were supported at the ends with the help of neoprene bearing pads, with the center of pads located 6-in from the end of the specimen to produce a 27-ft overall bending span. A two-point loading scheme was used at an equal distance of 3’3” from the splice section. The distance between the loads was determined to be 6’ 6” according to the spreader beam configuration available at the FDOT SRC laboratory.

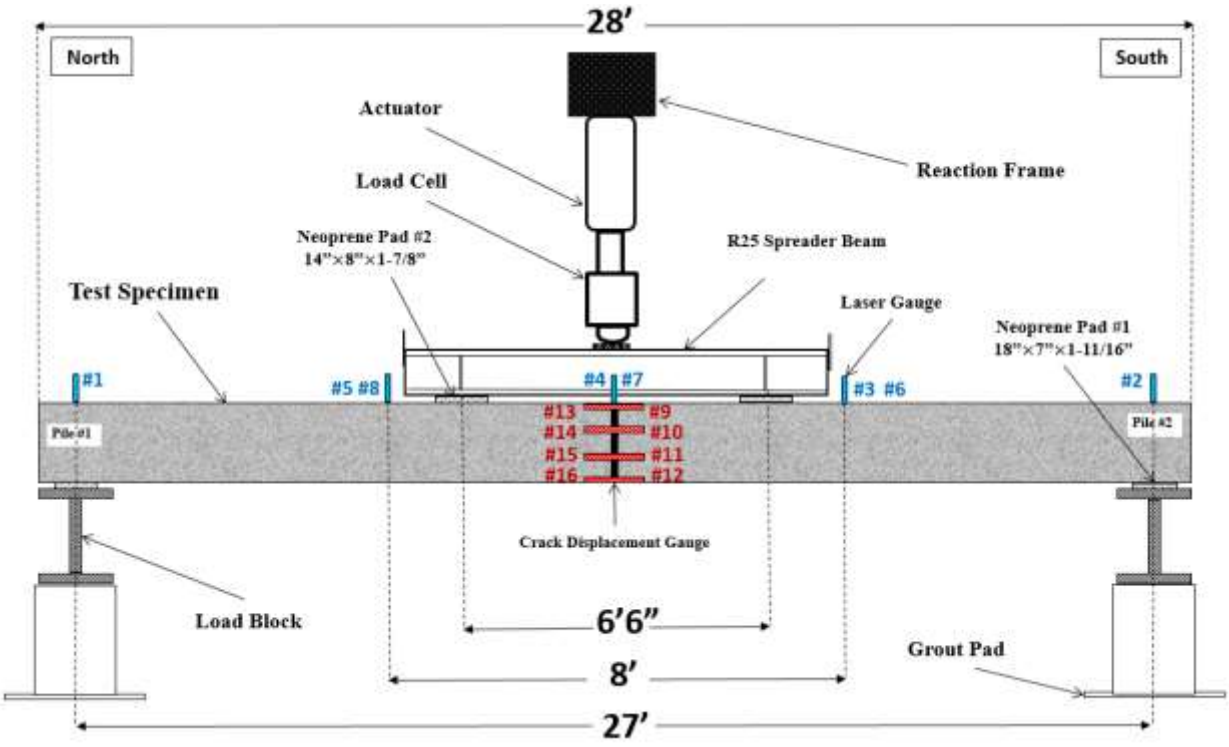

Figure 20: Instrumentation of the front view of test specimen

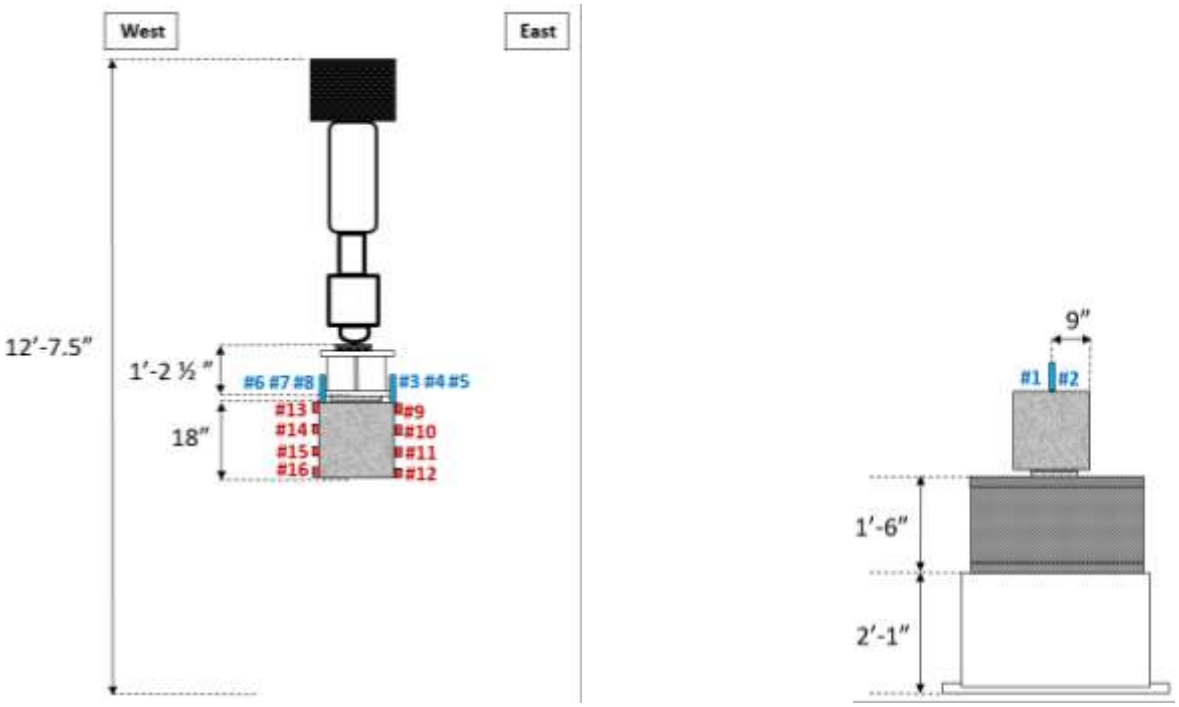

Figure 21: Instrumentation of the side view of test specimen at middle (left) and bottom (right) locations

Eight crack displacement transducers (#9 through #16 in Fig. 21), four on each face of specimen. with equal distance (5-in) were used to measure the potential crack development at the joint. Furthermore, six laser displacement sensors (#3 through #8 in Fig. 21) were installed on frames above the specimen and pointing to the top of the specimen. Two of these sensors were installed on both sides of the splice section, and four (two on each side) with a distance of 4 ft from the splice section. Two laser displacement (#1 and #2 in Figure 21), one at each end of the specimen were also installed pointing to the top of the specimen immediately over the bearing pads to measure any displacement at the support locations. This arrangement of the laser transducers was used to obtain the deflected shape of the pile during its loading.

4.2 Flexural Capacity of the Test Specimens

Figure 22 shows the moment diagram for a simply-supported beam with two-point loads, in which the maximum moment is expressed by Eq. (1).

$$M_{max} = \frac{P}{2} * a \quad (1)$$

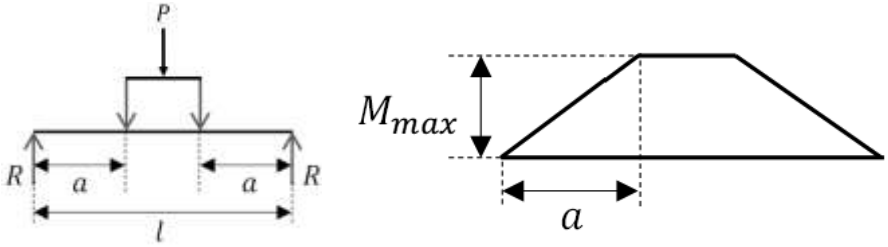

Figure 22: Moment diagram for two-point loading

The cracking moment was calculated to be 47.06 k-ft for an 18x18 in. pile section. To calculate the cracking load, the self-weight moment of the system must be subtracted from the cracking moment. The moment corresponding to self-weight of the pile is shown below.

$$W_{sw} = 2.25 \times 145 \text{ lb/ft}^3 = 326.25 \text{ lb/ft} \quad (2)$$

$$M_{sw} = \frac{\left(326.25 \frac{\text{lb}}{\text{ft}}\right)(27)^2}{8} = 29.7 \text{ k-ft} \quad (3)$$

The weight of the spreader beam that is below the load cell needs to be also considered. The moment added from the weight of the spreader beam is shown below.

$$M_{sb}=\frac{\left(109\,\frac{\text{lb}}{\text{ft}}\right)(8\text{ ft})(10.25\text{ ft})}{2} = 4.47\text{ k-ft} \quad (4)$$

Adding this moment to the moment from the self-weight of the specimen results in a total dead-weight moment of 34.17. This moment must be added to the moment from loading measured by the load cell to obtain the total moment capacity from testing.

The cracking load, P_{cr}, corresponds to cracking moment, M_{cr}, of the splice section. Using Eq. 5, the total applied load corresponding to the cracking moment is estimated to be 3.38 kips.

$$P_{cr} = \frac{2(Mcr-Msw)}{a} = \frac{2\times(47.06-34.17)}{10.25} = 2.51\text{ kips} \quad (5)$$

At the point of the cracking moment, the maximum tensile stress is considered to be f_t (Eq. 6).

$$f_t = 7.5\sqrt{f_c'} = \frac{7.5*\sqrt{6000}}{1000} = 0.581\text{ ksi} \quad (6)$$

To estimate the Ultimate Load, the maximum moment resistance calculated in Task 2 of this project was used. Maximum moment resistances (before application of the resistance factor) for various types of dowel material for 18x18-in. piles splices are listed in Table 8. To calculate the estimated ultimate load, the self-weight of the system must be added to the moment from the applied load and set equal to the estimated moment resistance.

$$P= \frac{2(Mn-Msw)}{a} \quad (7)$$

During the laboratory bending tests of the splice pile specimens, the average compressive strength of eighteen (18) cylindrical samples was obtained to be 7,336 psi (Appendix C). From section analysis of the test specimens, the nominal moment strength of the splice sections was calculated for both nominal concrete strength (6.5 ksi) and actual average concrete strength at the time of testing (7.3 ksi) using formulation developed in Task 2 and are included in Column 3 of Table 8. The ultimate loads corresponding to these moment capacities taking into account the self-weight were calculated and are shown in Column 4 of Table 8.

Table 8: Ultimate loads of the test specimens from section analysis

Dowel Material	Concrete Strength	Estimated Moment Resistance	Estimated Ultimate Load
GFRP	6.5 ksi	222.74 k-ft	36.79 kips
	7.3 ksi	233.26 k-ft	38.84 kips
CFRP	6.5 ksi	198.02 k-ft	31.97 kips
	7.3 ksi	207.2 k-ft	33.76 kips
Steel	6.5 ksi	305.1 k-ft	52.86 kips
	7.3 ksi	323.4 k-ft	56.43 kips

To have a better expectation from pile splice behavior in this laboratory test, the estimated deflections at failure were calculated for both steel- and FRP-based pile specimens (Table 9).

Table 9: Estimated deflection at failure of the test specimen

Dowel Material	Total Deflection		
Steel	Yield deflection = 3.01 “	Plastic Load = 0.158 “	Total= ~ 4“
FRP	Pre-crack Deflection = 0.64“	Post-crack Deflection = 4.92”	Total= ~ 6“

4.3 Loading Procedure

Three load levels were used as references during the flexural testing. The “Initial Loading” is a low-level loading that is used to set the test setup before taking initial readings of the instrumentation. The “Cracking Load” is a load level at which the first flexural cracking is expected to occur and the load-deflection curve deviates from the linear elastic (Figure 23). The “Ultimate Load” refers to the maximum load in flexural testing that corresponds to the Maximum Moment Resistance of the section.

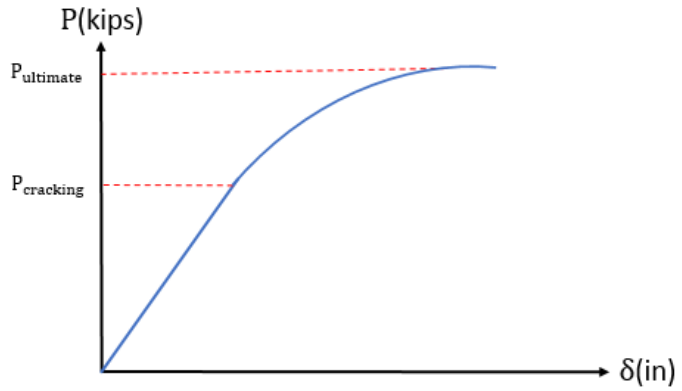

Figure 23: Schematic applied load against deflection in flexural testing

A 1-kip load was initially applied and removed to set the supports. Initial readings were taken at this interval. Then, the applied load was increased at stages with different load rates and intervals to investigate the cracking and failure load and deflection at pile splice, as shown in Tables 10 and 11. The specimens were inspected at each load interval, cracks were mapped and photos were taken.

Table 10: Loading details for test specimens using GFRP and CFRP Dowels (Specimens 1, 2, 3, 4, 5, 6, 9, and 10)

Steps	Start Load	End Load	Load Rate
Initial Loading	0 kips	1 kips	150 lbs/s
Initial Loading	1 kips	0 kips	150 lbs/s
1	0 kips	5 kips	150 lbs/s
2	5 kips	10 kips	100 lbs/s
3	10 kips	20 kips (Gauge Removal)	100 lbs/s
4	20 kips	Failure Load	100 lbs/s

Table 11: Loading details for test specimens using Steel Dowel (Specimens 7 and 8)

Steps	Start Load	End Load	Load Rate
Initial Loading	0 kips	1 kips	150 lbs/s
Initial Loading	1 kips	0 kips	150 lbs/s
1	0 kips	5 kips	150 lbs/s
2	5 kips	10 kips	100 lbs/s
3	10 kips	20 kips	100 lbs/s
4	20 kips	30 kips (Gauge Removal)	100 lbs/s
5	30 kips	Failure Load	100 lbs/s

5 EXPERIMENTAL TEST RESULTS

This chapter reports the results that were obtained from the experimental test performed at the FDOT structures lab based on the proposed experimental program. The main purpose of this experimental program was to determine the flexural strength of different pile splices. Another purpose was to determine the development length of the proposed FRP dowels. Figure 24 shows the test setup with a spliced pile specimen.

Figure 24: The test setup

As shown in Figure 25, for each specimen, an inspection sheet was filled out in detail, and the specimens were photographed. The experimental program was scheduled to test about one pile per day during a two-week time period. Before the experimental test, all pile specimens were inspected for cracks, debonding, and spalling caused by shipping. Data from instrumentations were collected at an acceptable frequency, e.g., 10 per second, and stored in a data acquisition system. According to the loading procedure, the test was paused at each loading interval to inspect the specimen for cracks, openings and other events. The cracks and openings were traced and marked with an identifying designation. Photographs were taken at the end of each pause. The entire test process was videotaped.

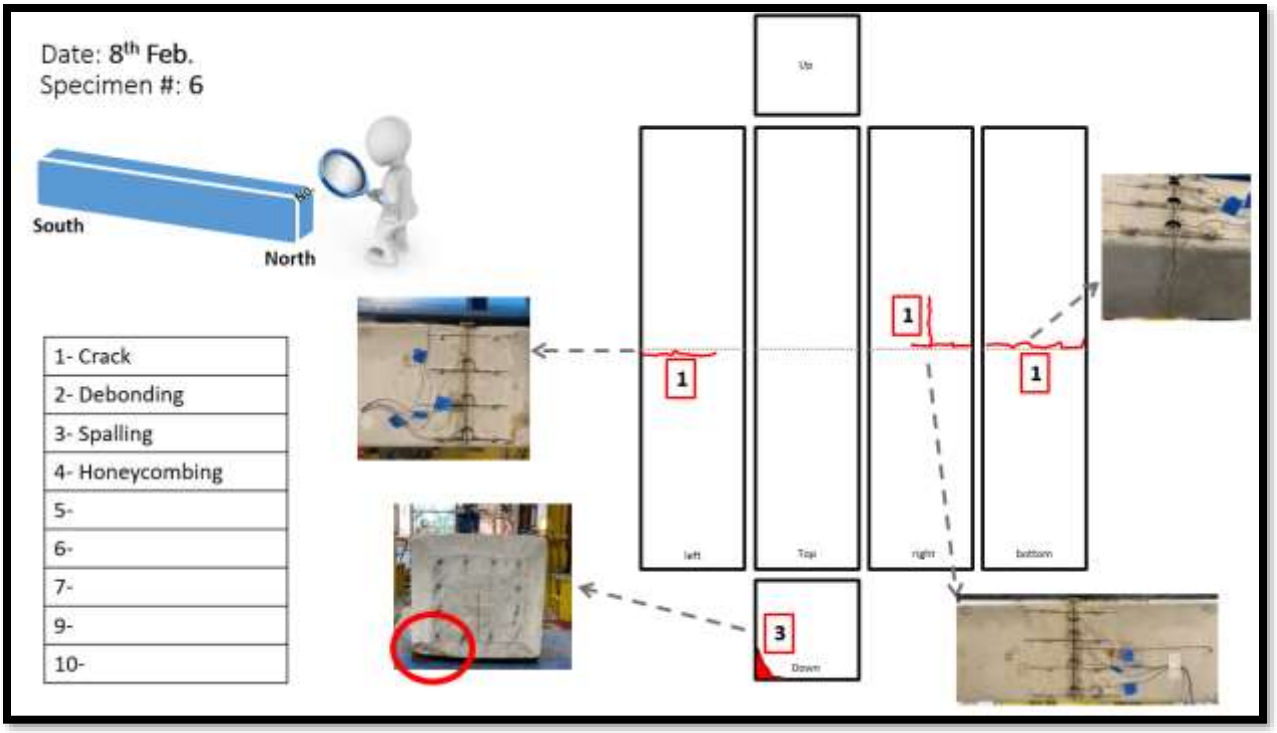

Figure 25: An example of the inspection sheet

After the completion of each test, the data was processed to obtain plots for:

- **Load-displacement**: In this plot, deflection is the average of readings from Gauges #4 and #7 (at mid span), minus the average of readings from Gauges #1 and #2 (at two ends) (Figure 20). The load is the reading from the load cell.
- **Load-deflection profile:** The average of readings from Gauges #3 and #6, #4 and #7, and #5 and #8, minus the average of readings from Gauges #1 and #2, provides the deflection profile of the specimen.
- **Crack-opening profile:** In this plot, the crack opening over the section depth of the pile splice is the average of readings from Gauges #9 and #13, #10 and #14, #11 and #15, and #12 and #16 (Figure 20).
- **Load-crack opening**: This plot shows the crack-opening behavior of the pile splice corresponding to the average of readings from Gauges #9 and #13 (Level 1), #10 and #14 (Level 2), #11 and #15 (Level 3), and #12 and #16 (Level 4).

5.1 Specimen 1

In Specimen 1, a crack was observed in the splice section prior to the test setup. In this test, the first new flexural crack was observed at the splice section at Step 1, load ≤ 5 kips. Moreover, the first splitting crack (near-horizontal crack) was detected at Step 2 (load ≤10 kips) at the level of the lowest set of strands. As the load increased, more splitting cracks developed on both sides of the splice section at the level of the lowest strand and midsection. These cracks extended farther until the specimen reached its maximum load at 28.09 kips with concrete crushing at the top of the section in the female segment, 2 ft from the splice section. This is in the proximity of the end of the dowel's length (2ft, 6in.). Prior to the concrete crushing, horizontal and vertical cracks showed large openings consistent with splitting due to bond failure. Figure 26 shows the failure mode and crack pattern for this test specimen. The maximum moment capacity was calculated for this specimen to be 178.13 k-ft, taking into account the moment from the self-weight of the specimen and the spreader beam. Dissection after testing showed that there is no major misalignment with the holes drilled in the female segment and their corresponding dowels in the male segment (Figure 27).

Figure 26: Crack propagation and failure mode of Specimen 1

Figure 27: A photo of the Specimen 1 after test

For Specimen 1, the load-displacement curve, load-deflection profile, crack-opening profile, and load-crack opening curve were plotted, as shown in Figures 28-31, respectively.

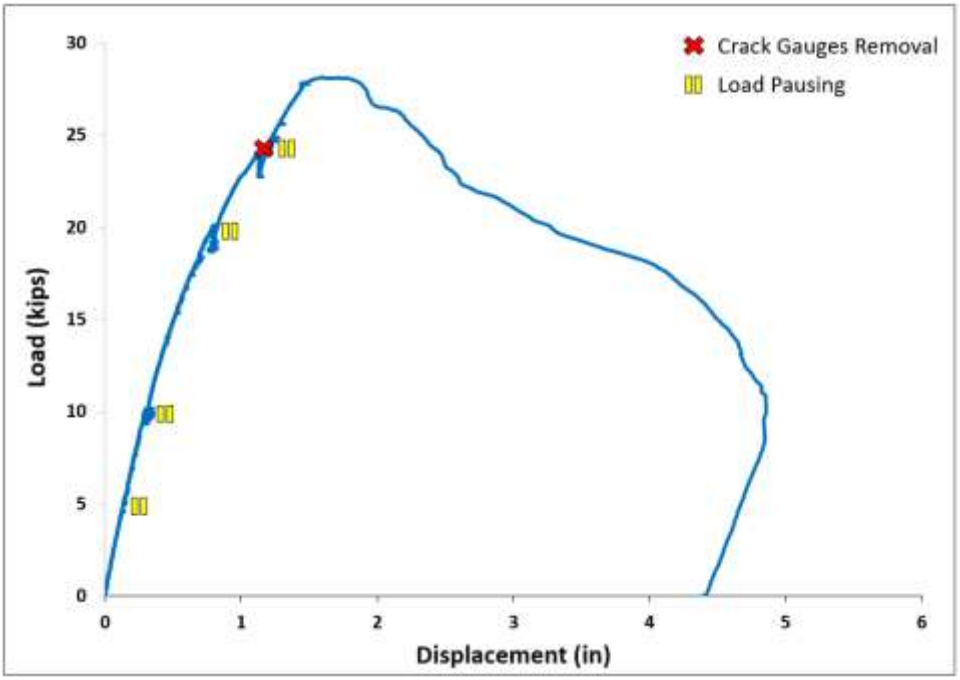

Figure 28: Load-displacement curve for Specimen 1

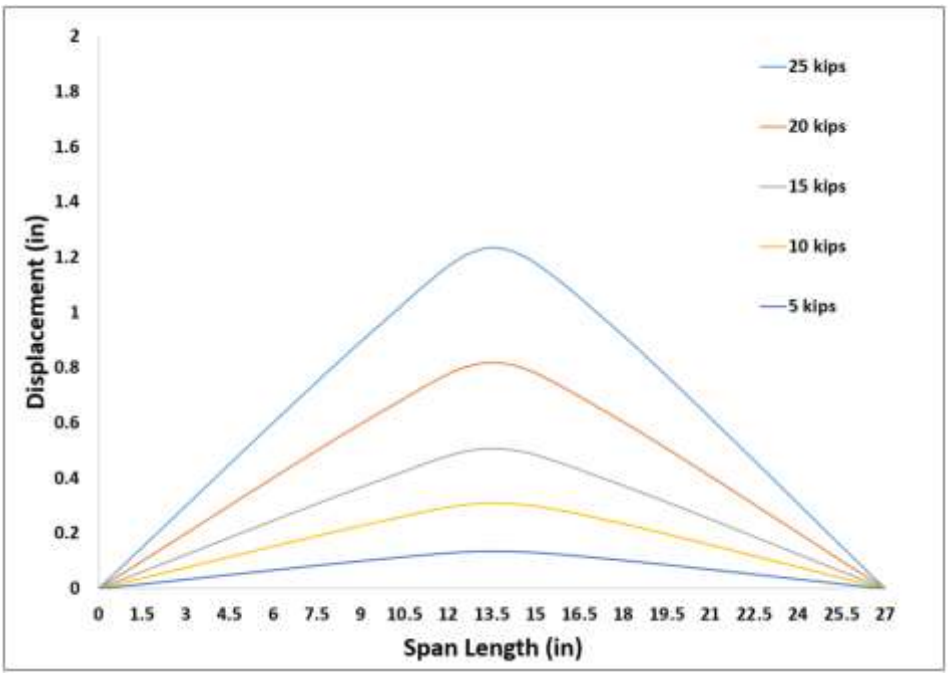

Figure 29: Load-deflection profile for Specimen 1

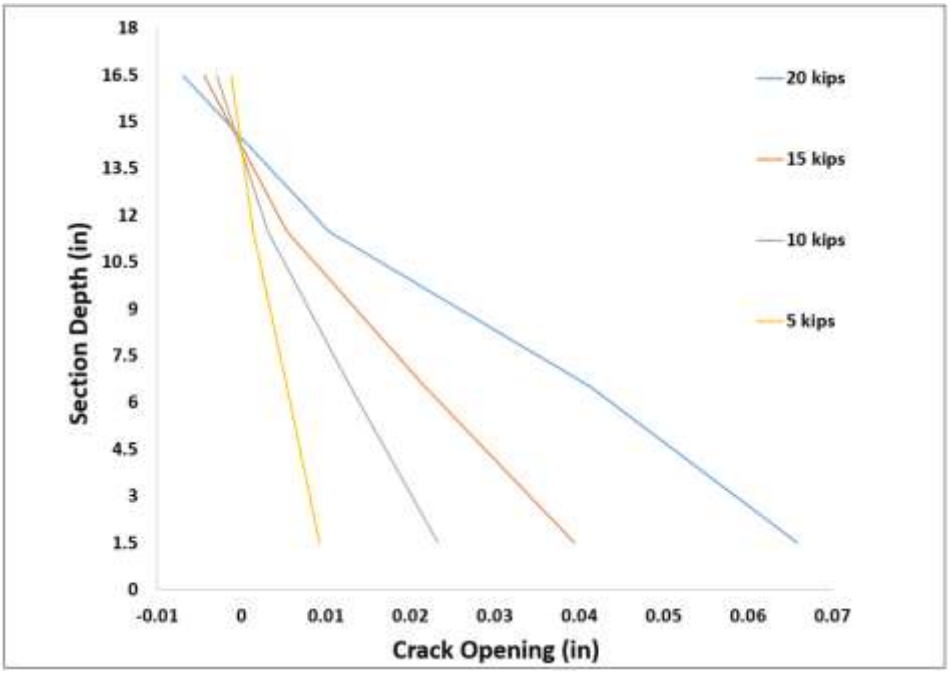

Figure 30: Crack-opening profile for Specimen 1

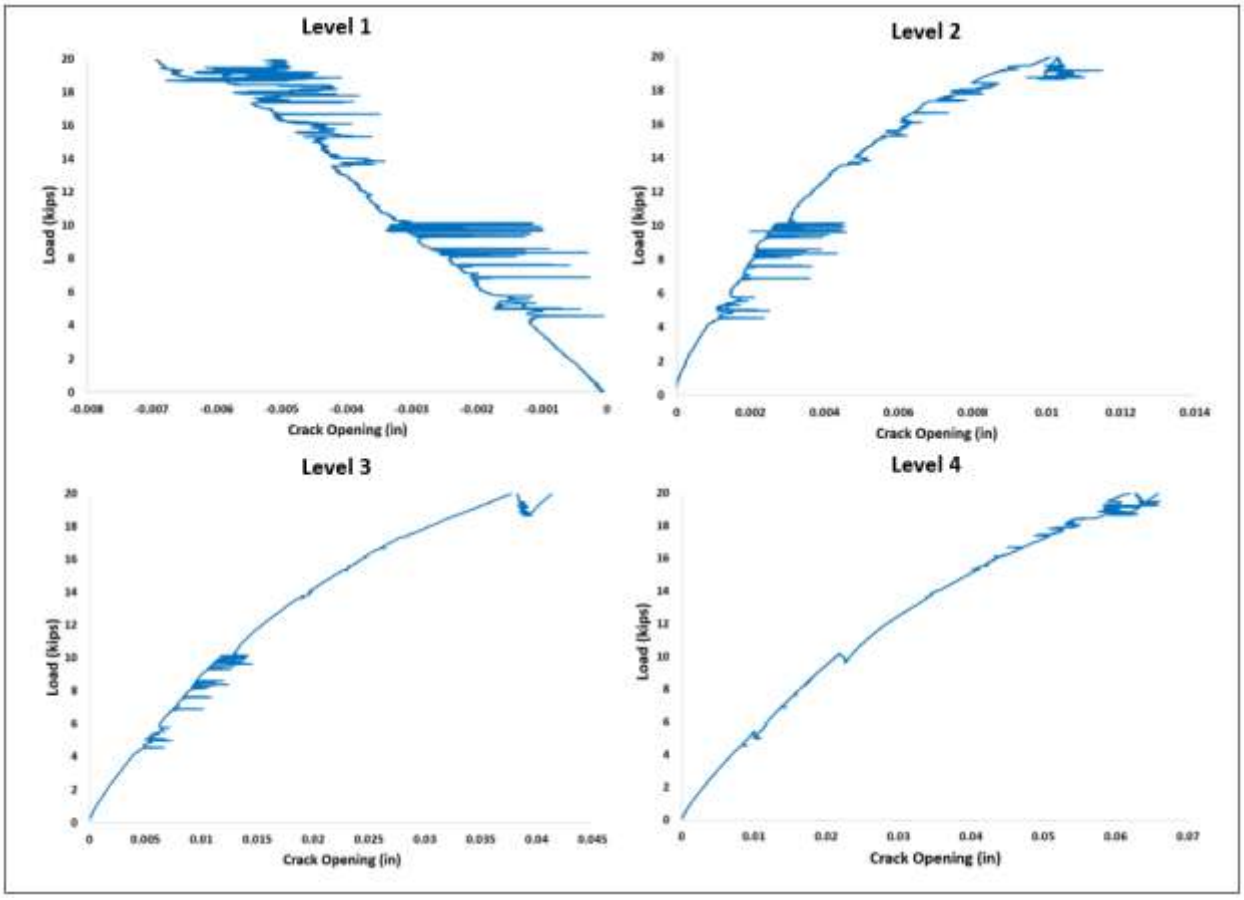

Figure 31: Load-crack opening curves for Specimen 1

5.2 Specimen 2

In Specimen 2, a crack was observed in the splice section prior to the test setup. In this test, the first new flexural crack was observed in the splice section at Step 1, load ≤ 5 kips. Moreover, the first splitting crack was detected at Step 2 (load ≤10 kips) at the second level of strands from the top, the second level of strands from the bottom, and at the midsection level. As the load increased, additional splitting cracks developed on both sides of the splice section. These cracks extended farther until the specimen reached its maximum load at 20.53 kips with a large opening consistent with splitting due to bond failure at the bottom of the section in the female segment. Figure 32 shows the failure mode and crack pattern for this test specimen. The maximum moment capacity was calculated for this specimen to be 139.38 k-ft, taking into account the moment from the self-weight of the specimen and the spreader beam.

Figure 32: Crack propagation and failure mode of Specimen 2

Dissection after testing revealed some issues with the holes drilled in the female segment to receive the dowels. Apparently, secondary drilling was performed to align with the dowels. Figure 33 shows the oversized slanted hole. It is also clear from this figure that the splitting cracks in concrete have bridged the oversized hole, likely resulting in lower over strength for the specimen.

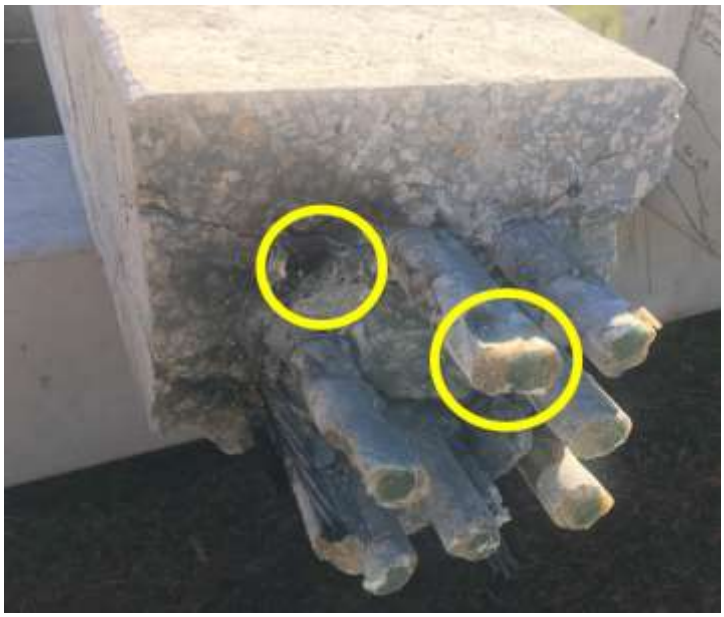

Figure 33: The oversized slanted holes

For Specimen 2, the load-displacement curve, load-deflection profile, crack-opening profile, and load-crack opening curve were plotted, as shown in Figures 34-37, respectively.

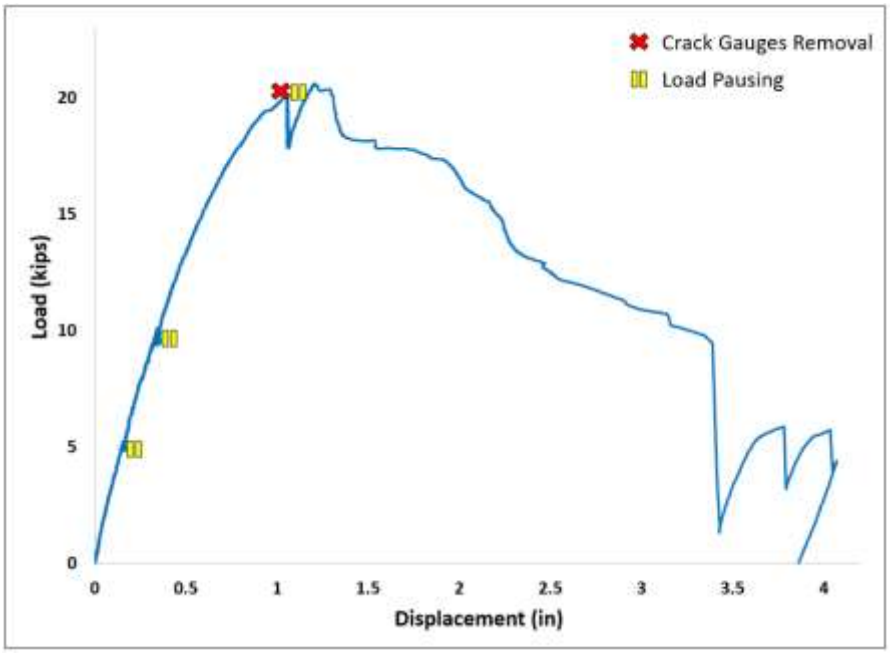

Figure 34: Load-displacement curve for Specimen 2

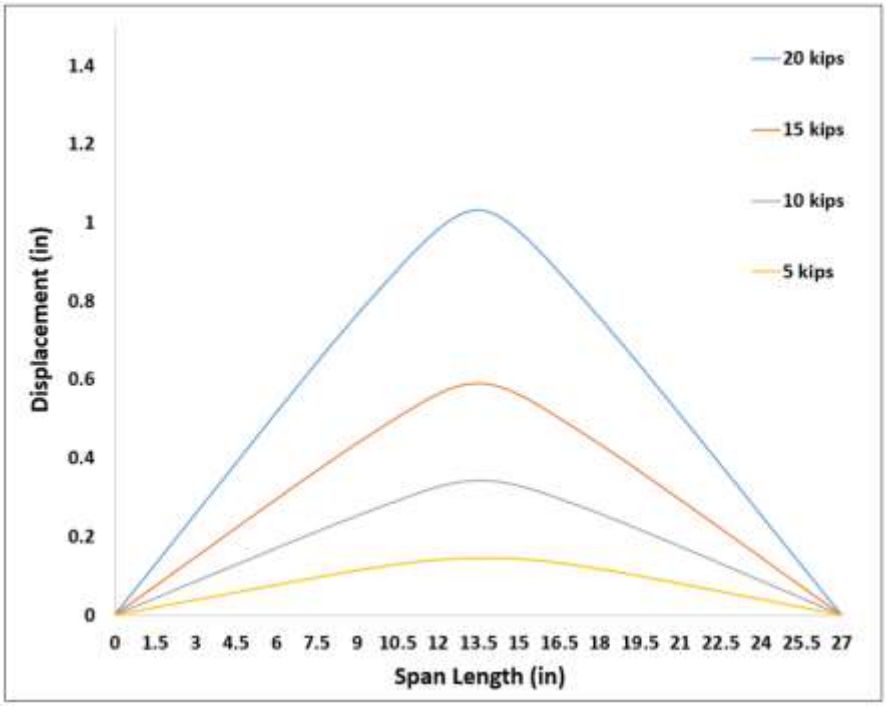

Figure 35: Load-deflection profile for Specimen 2

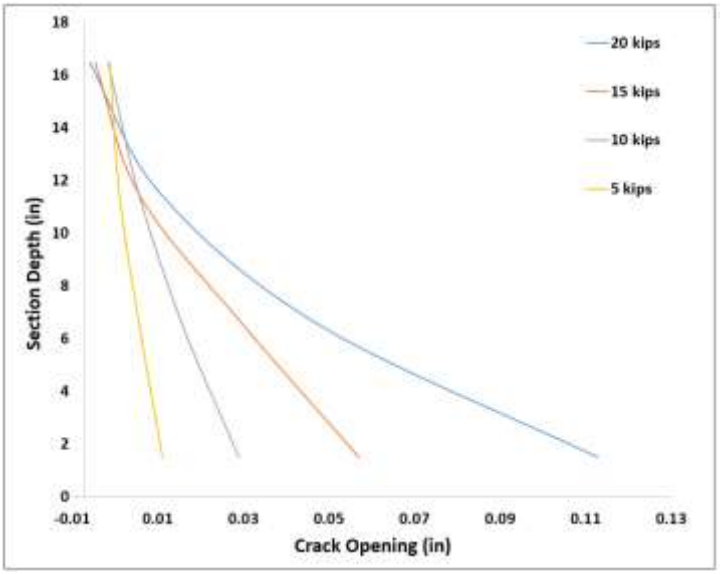

Figure 36: Crack-opening profile for Specimen 2

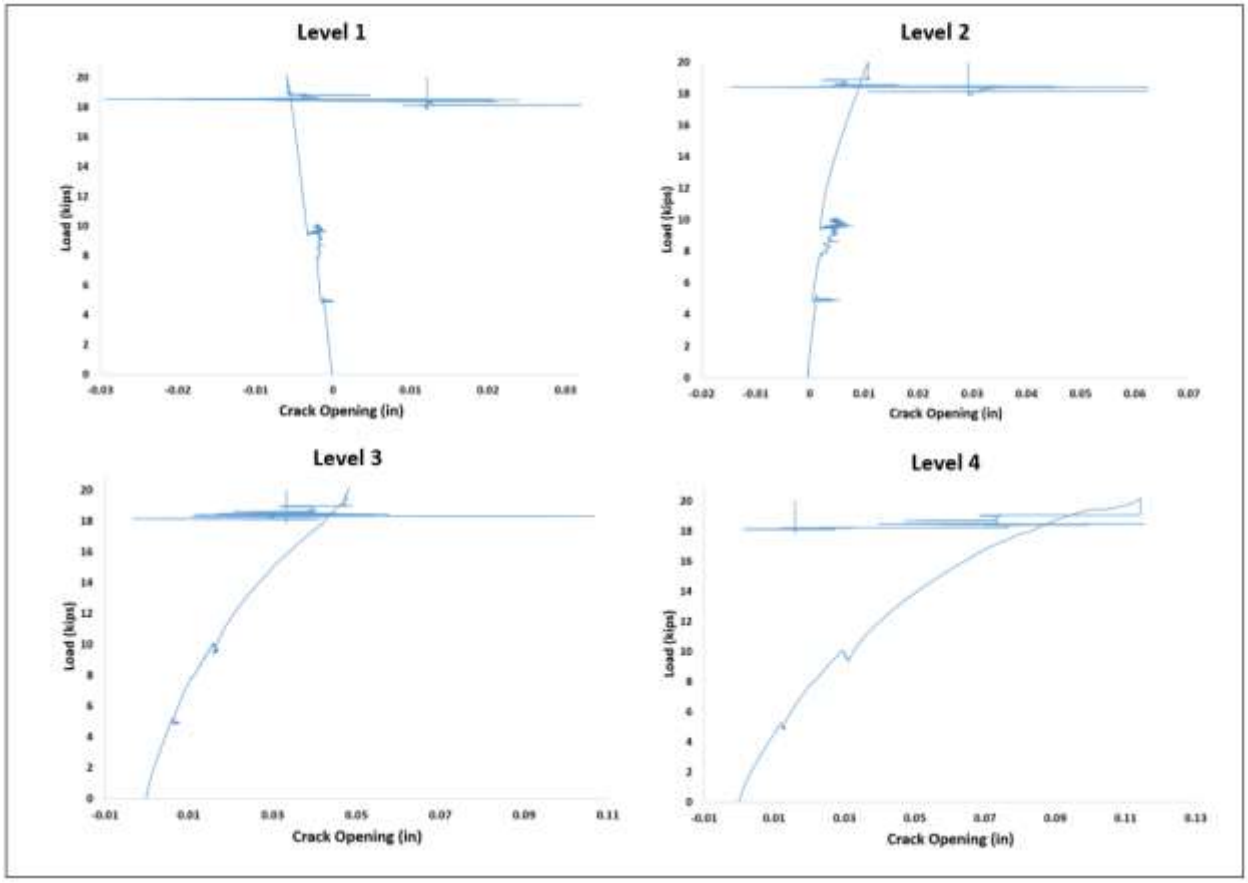

Figure 37: Load-crack opening curves for Specimen 2

5.3 Specimen 3

In Specimen 3, a crack was observed in the splice section prior to the test setup. In this test, the first new flexural crack was observed in the splice section at Step 1, load ≤ 5 kips. Moreover, the first splitting crack was detected at Step 2 (load ≤10 kips) at the first and second levels of strands from the bottom of the section. As the load increased, additional splitting cracks developed on both sides of the splice section. These cracks extended farther until the specimen failed at 41.72 kips with concrete crushing at the top of the pile at the splice section. Figure 38 shows the failure mode and crack pattern for this test specimen. The maximum moment capacity was calculated for this specimen to be 247.98 k-ft, taking into account the moment from the self-weight of the specimen and the spreader beam.

Figure 38: Crack propagation and failure mode of Specimen 3

For Specimen 3, the load-displacement curve, load-deflection profile, crack-opening profile, and load-crack opening curve were plotted, as shown in Figures 39-42, respectively.

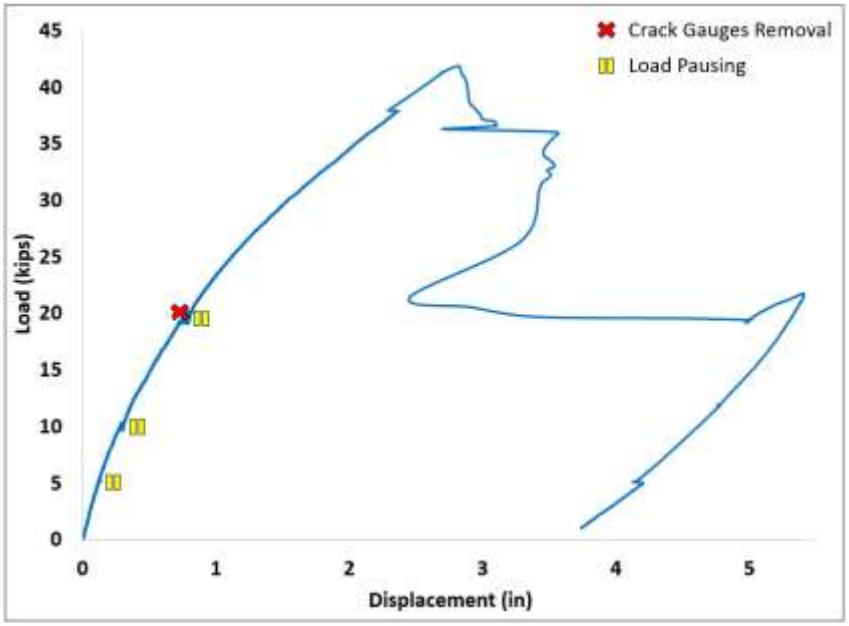

Figure 39: Load-displacement curve for Specimen 3

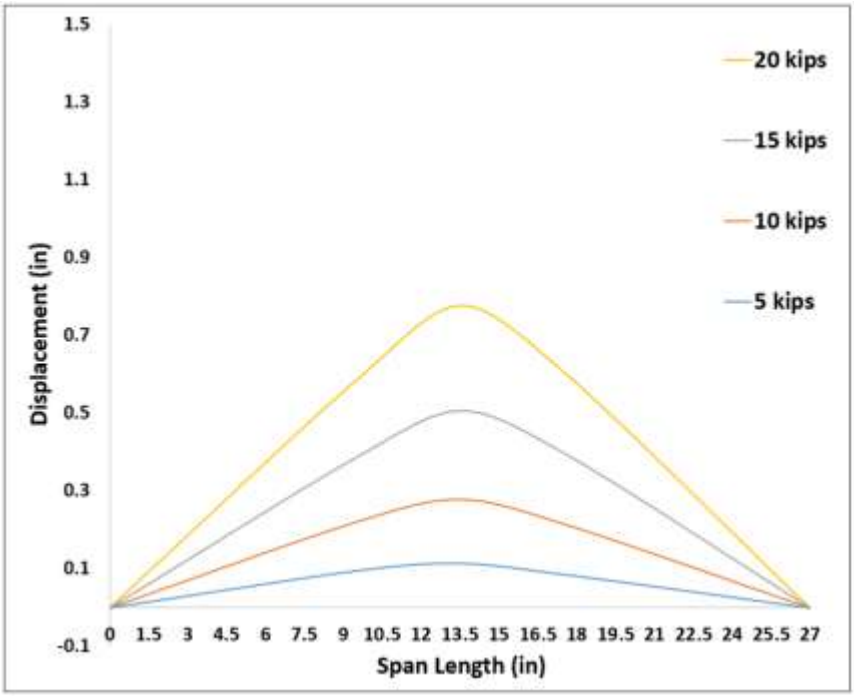

Figure 40: Load-deflection profile for Specimen 3

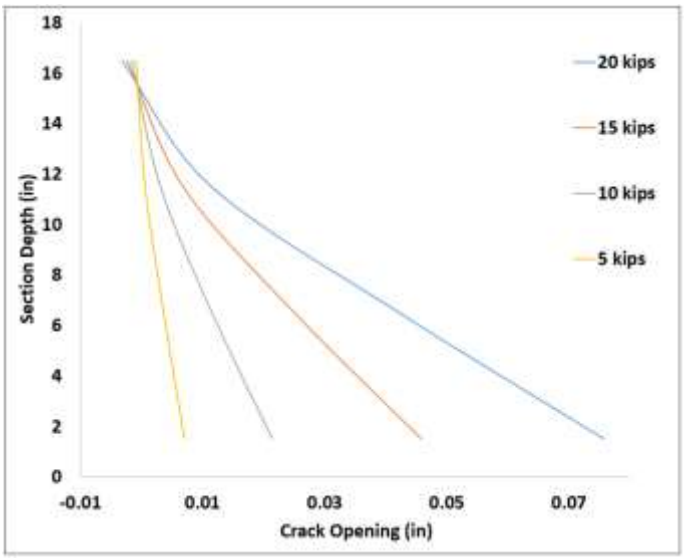

Figure 41: Crack-opening profile for Specimen 3

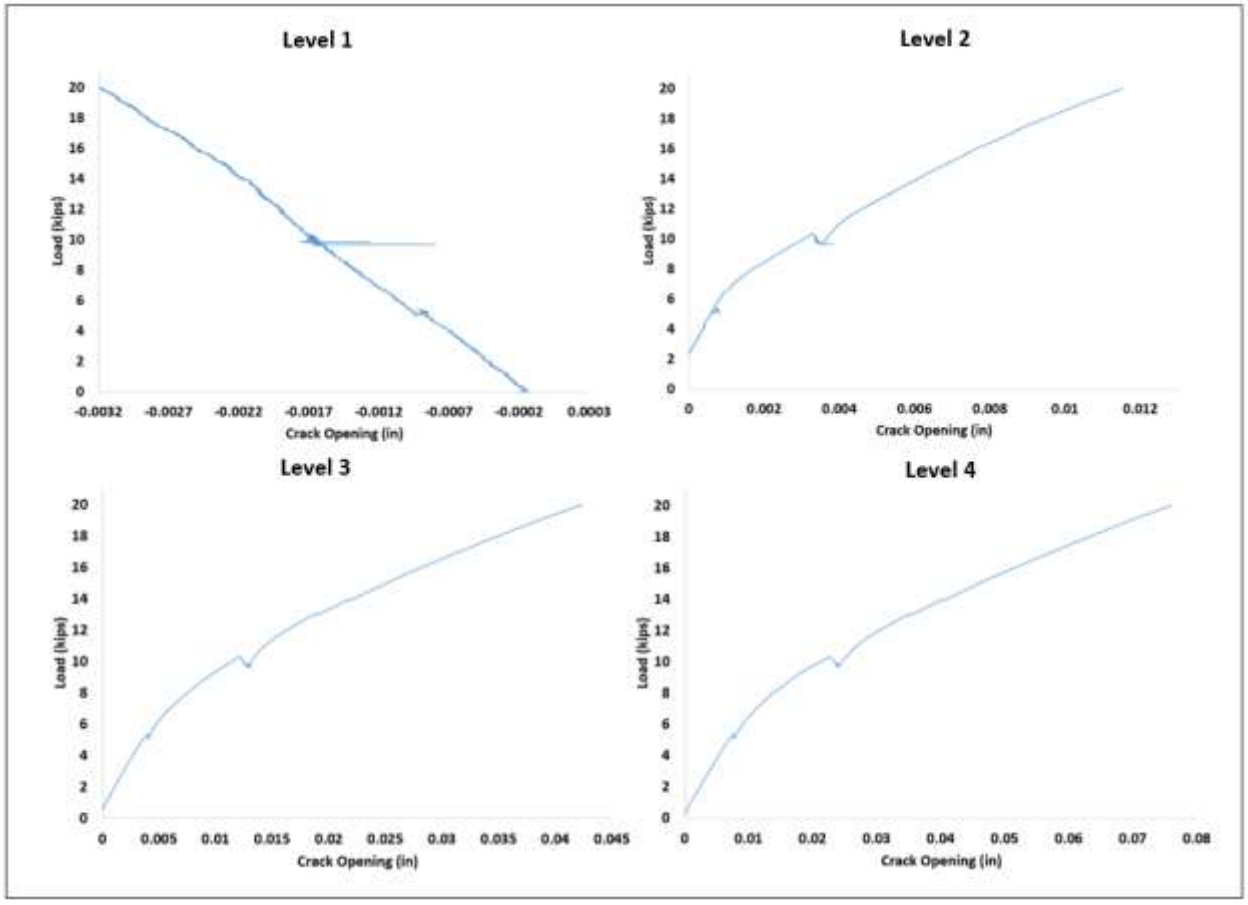

Figure 42: Load-crack opening curves for Specimen 3

5.4 Specimen 4

In this specimen, a crack was observed in the splice section prior to the test setup. In this test, the first new flexural crack was observed in the splice section at Step 1, load $\leq$ 5 kips. Moreover, the first splitting crack was detected at Step 2 (load $\leq$10 kips) at the second level of strands from the bottom of the section. As the load increased, additional splitting cracks developed on both sides of the splice section. These cracks extended farther until the specimen failed at 41.26 kips with concrete crushing at the top of the pile at the splice section. Figure 43 shows the failure mode and crack pattern for this test specimen. The maximum moment capacity was calculated for this specimen to be 245.62 k-ft, taking into account the moment from the self-weight of the specimen and the spreader beam.

Figure 43: Crack propagation and failure mode of Specimen 4

For Specimen 4, the load-displacement curve, load-deflection profile, crack-opening profile, and load-crack opening curve were plotted as shown in Figures 44-47, respectively.

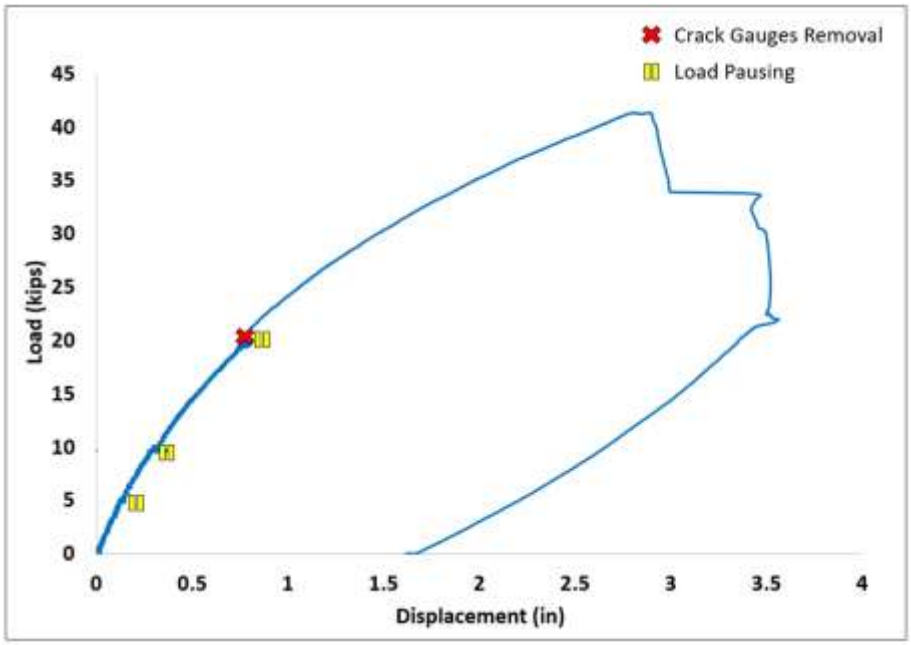

Figure 44: Load-displacement curve for Specimen 4

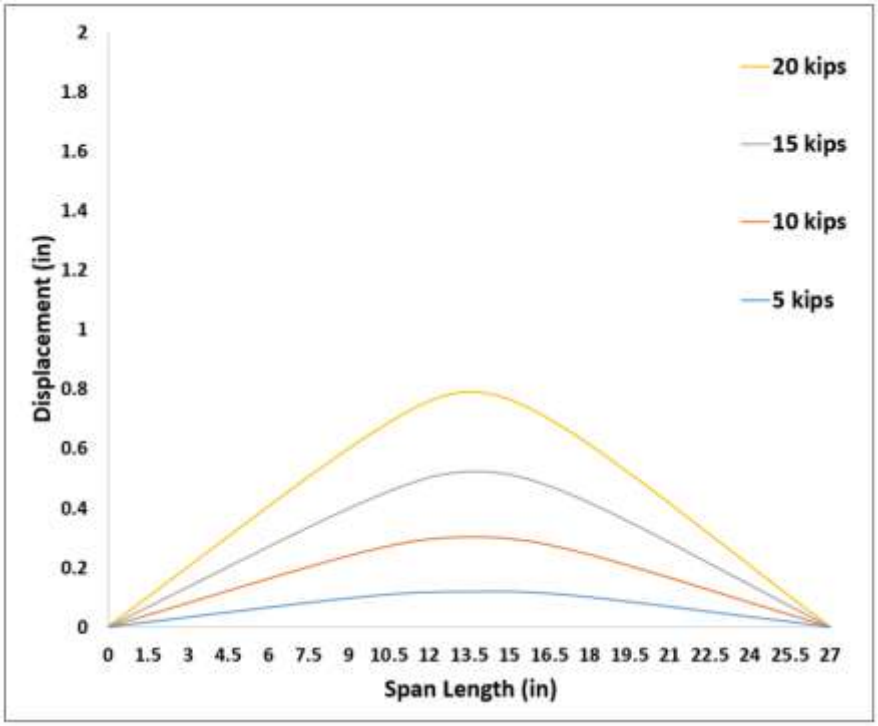

Figure 45: Load-deflection profile for Specimen 4

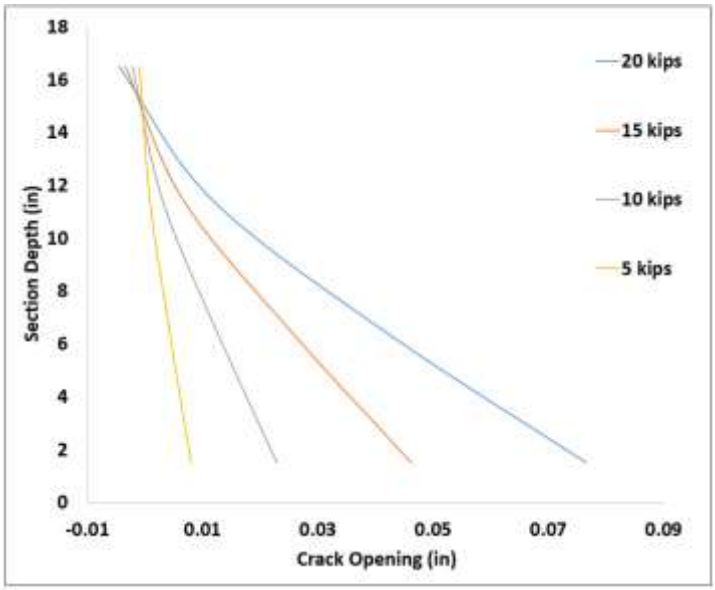

Figure 46: Crack-opening profile for Specimen 4

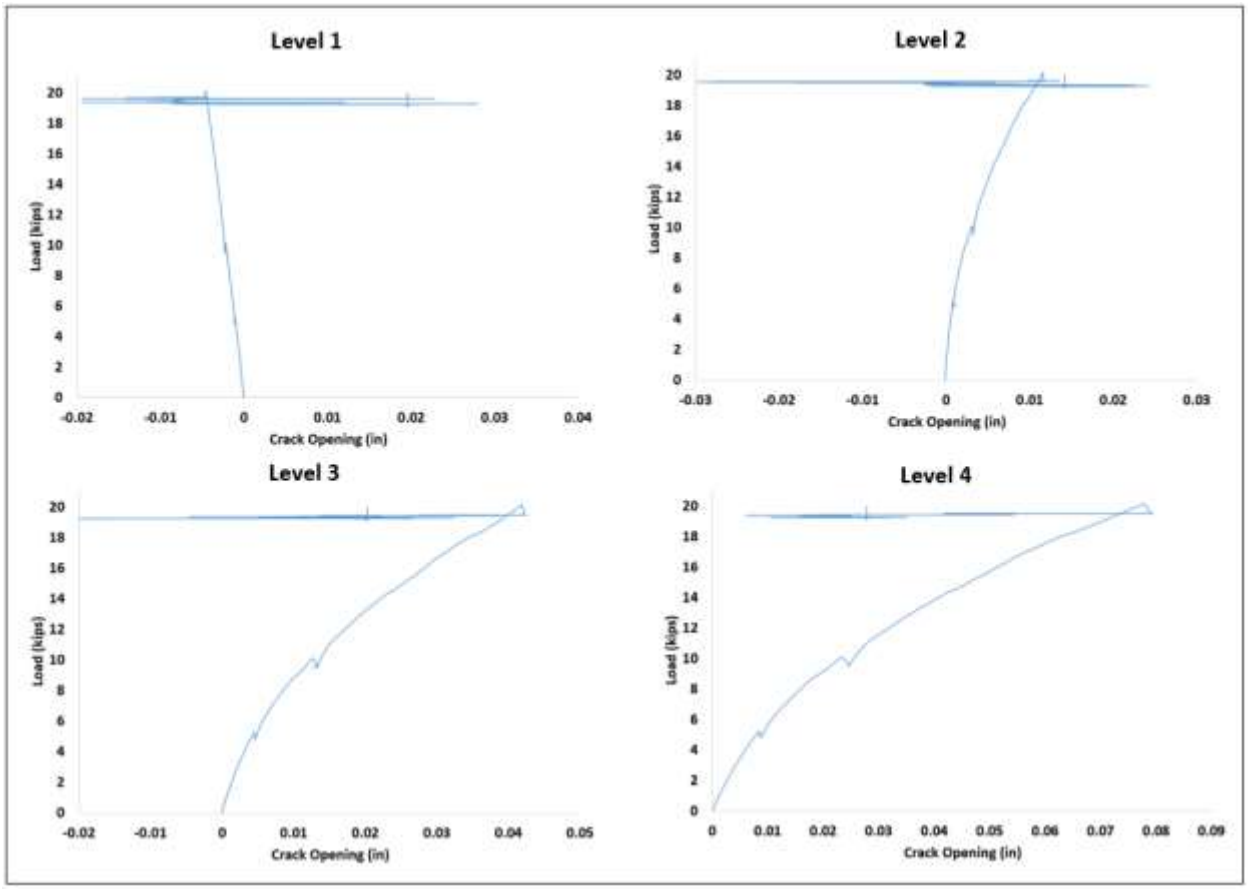

Figure 47: Load-crack opening curves for Specimen 4

5.5 Specimen 5

In Specimen 5, a crack was observed in the splice section prior to the test setup. In this test, the first splitting crack was detected at Step 1 (load $\leq$ 5 kips) in the midsection. Moreover, the first flexural crack was observed in the splice section at Step 2 (load $\leq$10 kips). As the load increased, additional splitting cracks developed on both sides of the splice section. These cracks extended farther until the specimen failed at 44.66 kips with a large opening in the male segment, 4ft and 6in from the splice section, which is in the proximity of the end of the dowel's length. The test was continued until the concrete crushed at the top of the section in the male segment at 29.95 kips. Figure 48 shows the failure mode and crack pattern for this test specimen. The maximum moment capacity was calculated for this specimen to be 263.05 k-ft, taking into account the moment from the self-weight of the specimen and the spreader beam.

Figure 48: Crack propagation and failure mode of Specimen 5

For Specimen 5, the load-displacement curve, load-deflection profile, crack-opening profile, and load-crack opening curve were plotted, as shown in Figures 49-52, respectively.

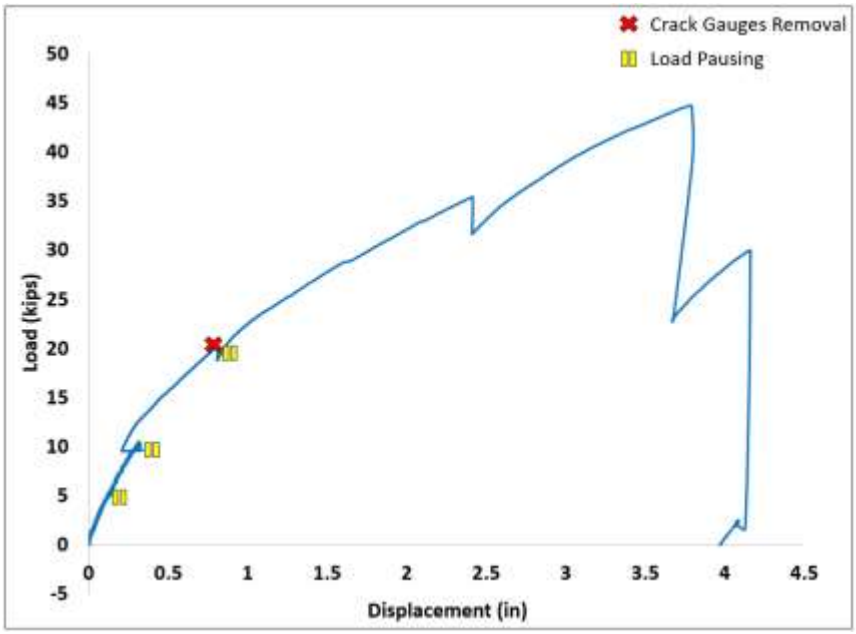

Figure 49: Load-displacement curve for Specimen 5

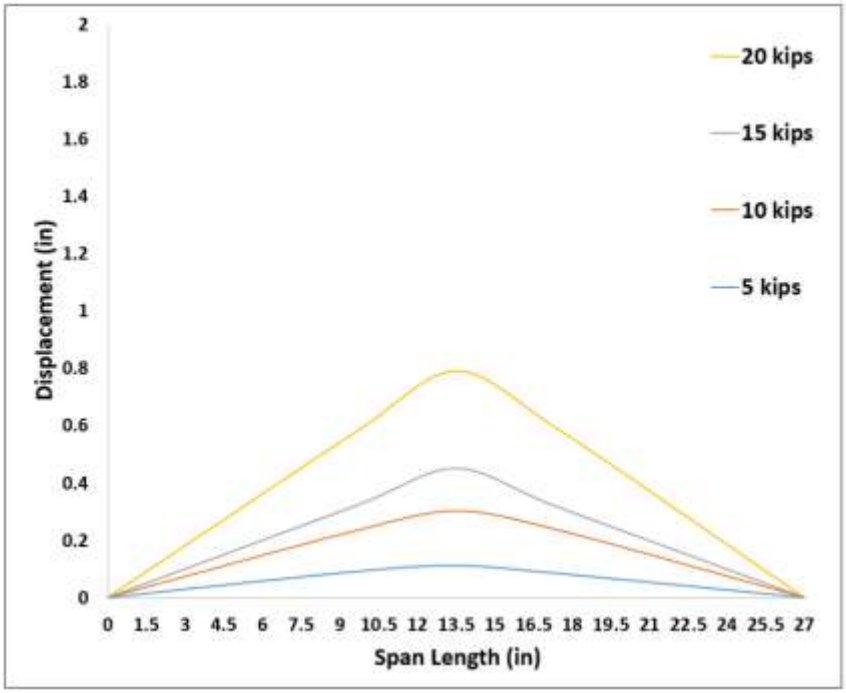

Figure 50: Load-deflection profile for Specimen 5

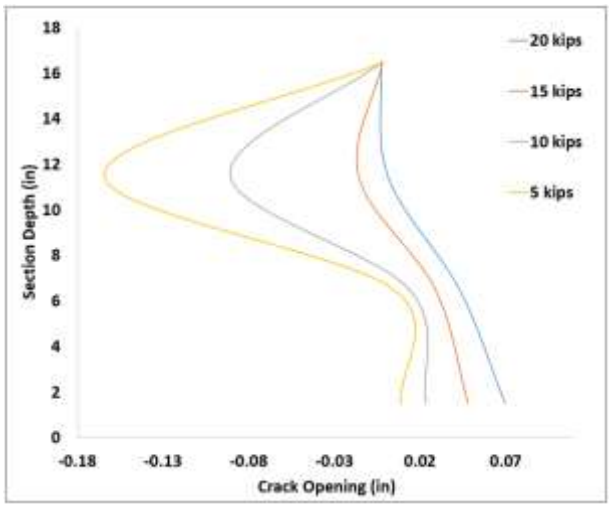

Figure 51: Crack-opening profile for Specimen 5

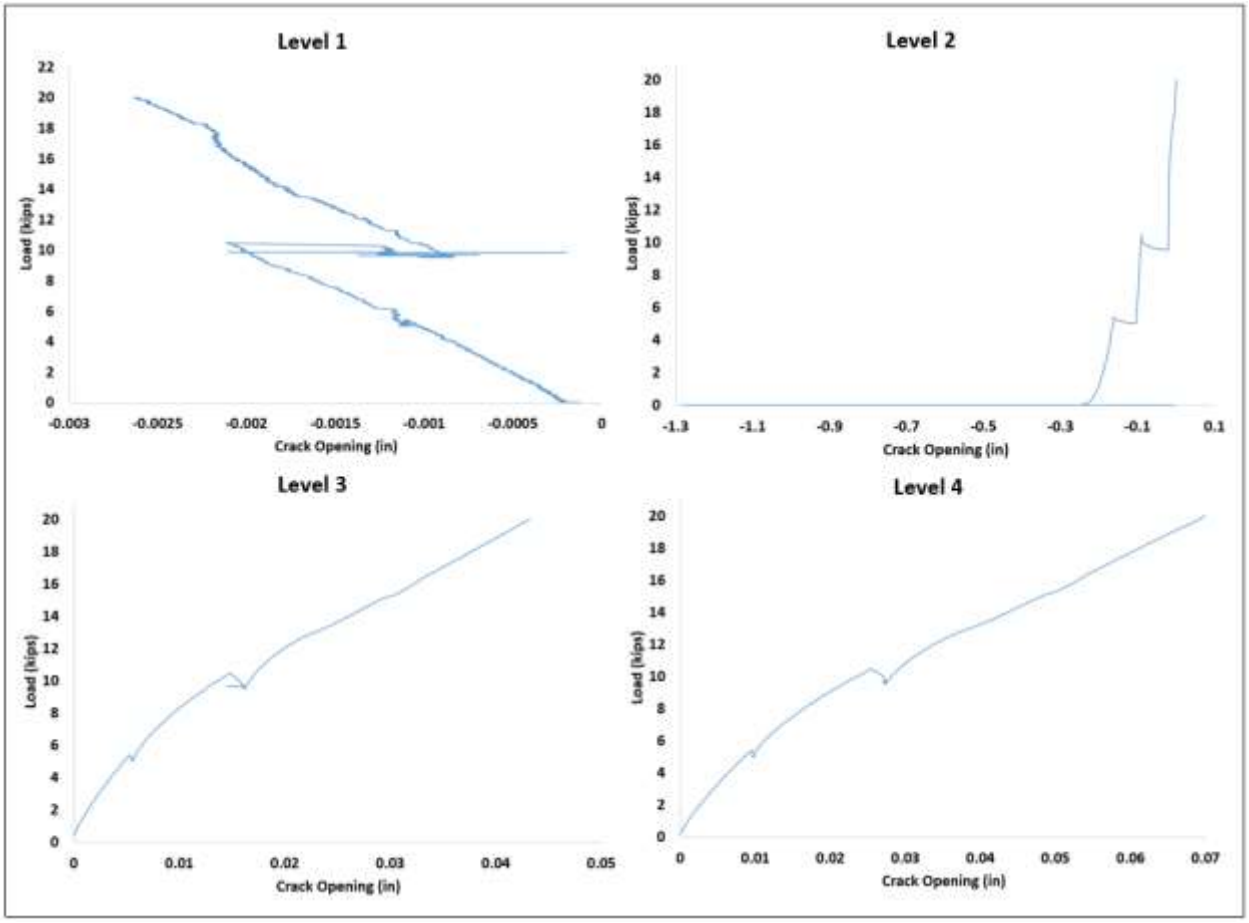

Figure 52: Load-crack opening curves for Specimen 5

5.6 Specimen 6

In this specimen, a crack was observed in the splice section prior to the test setup. In this test, the first splitting crack was detected at Step 2 (load ≤10 kips) in the upper level of the dowel and the second level of strands from the top of the section. As the load increased, additional splitting cracks developed on both sides of the splice section. These cracks extended farther until the specimen failed at 43.59 kips with a large opening in the male segment at 4ft and 6in from the splice section, which is in the proximity of the end of the dowel's length. The test was continued until the concrete crushed at the top of the section in the male segment at 30.91 kips. Figure 53 shows the failure mode and crack pattern for this test specimen. The maximum moment capacity was calculated for this specimen to be 257.57 k-ft, taking into account the moment from the self-weight of the specimen and the spreader beam.

Figure 53: Crack propagation and failure mode of Specimen 6

For Specimen 6, the load-displacement curve, load-deflection profile, crack-opening profile, and load-crack opening curve were plotted as shown in Figures 54-57, respectively.

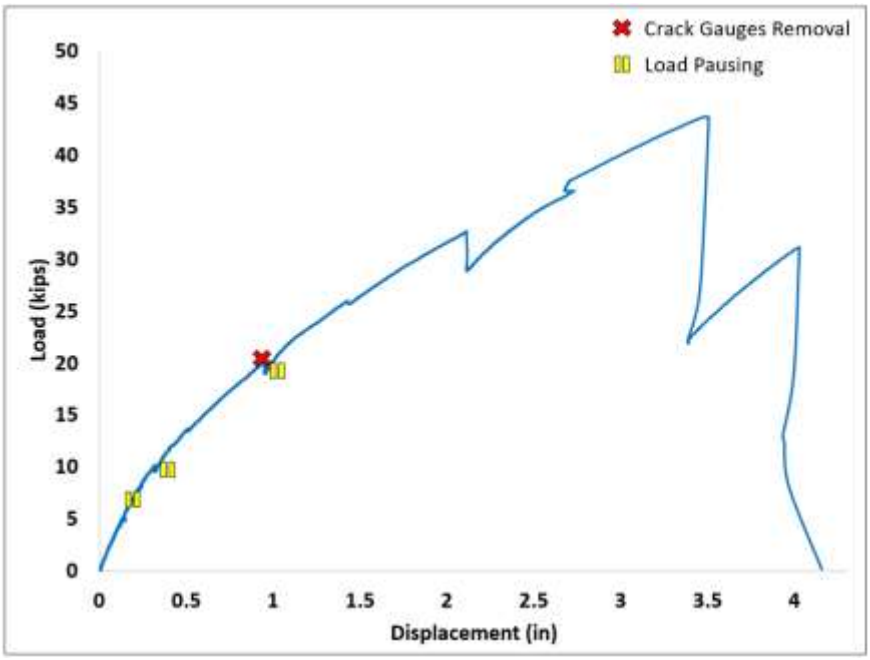

Figure 54: Load-displacement curve for Specimen 6

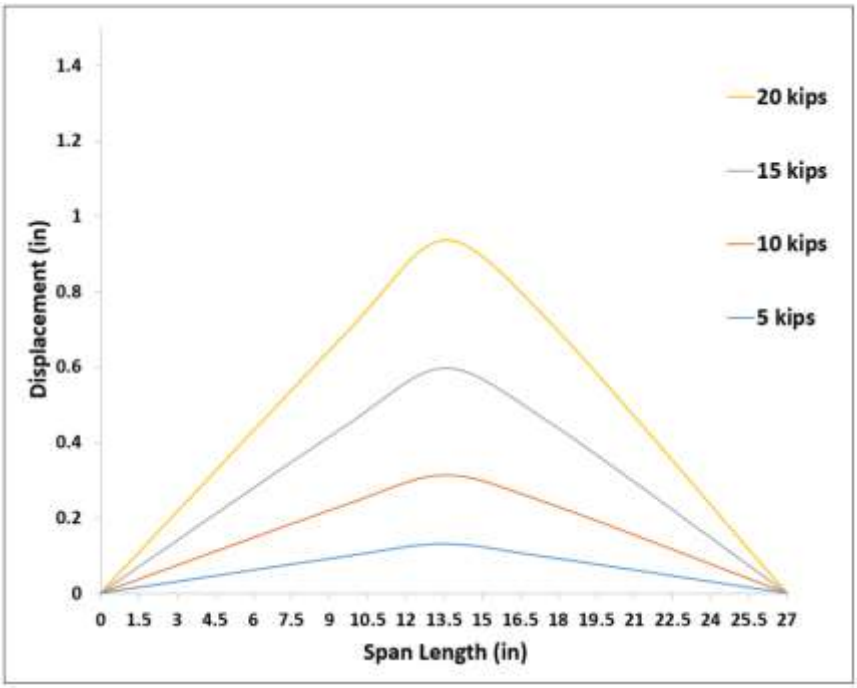

Figure 55: Load-deflection profile for Specimen 6

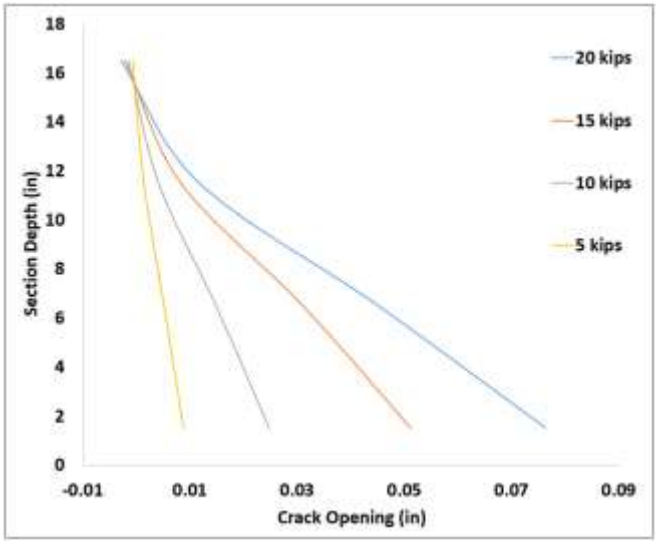

Figure 56: Crack-opening profile for Specimen 6

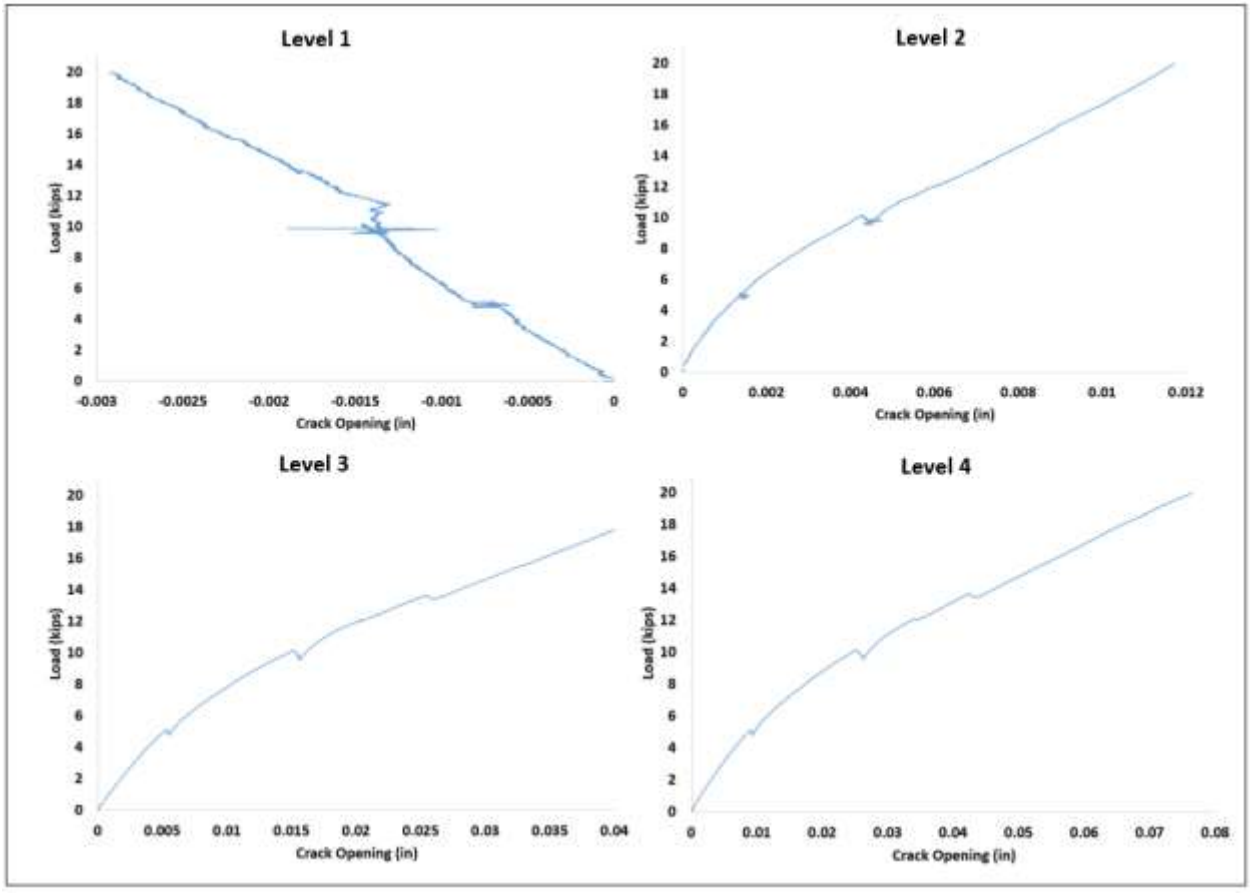

Figure 57: Load-crack opening curves for Specimen 6

5.7 Specimen 7

In this specimen, a crack was observed in the splice section prior to the test setup. In this test, the first new flexural crack was observed in the splice section at Step 2 (load ≤10 kips). Moreover, the first splitting crack was detected at Step 3 (load ≤20 kips) at the first and second levels of the strands from the bottom of the section. As the load increased, additional splitting cracks developed on both sides of the splice section. These cracks extended farther until the specimen failed at 61.17 kips with the concrete crushing at the top of the pile near the splice section. Figure 58 shows the failure mode and crack pattern for this test specimen. The maximum moment capacity was calculated for this specimen to be 347.67 k-ft, taking into account the moment from the self-weight of the specimen and the spreader beam.

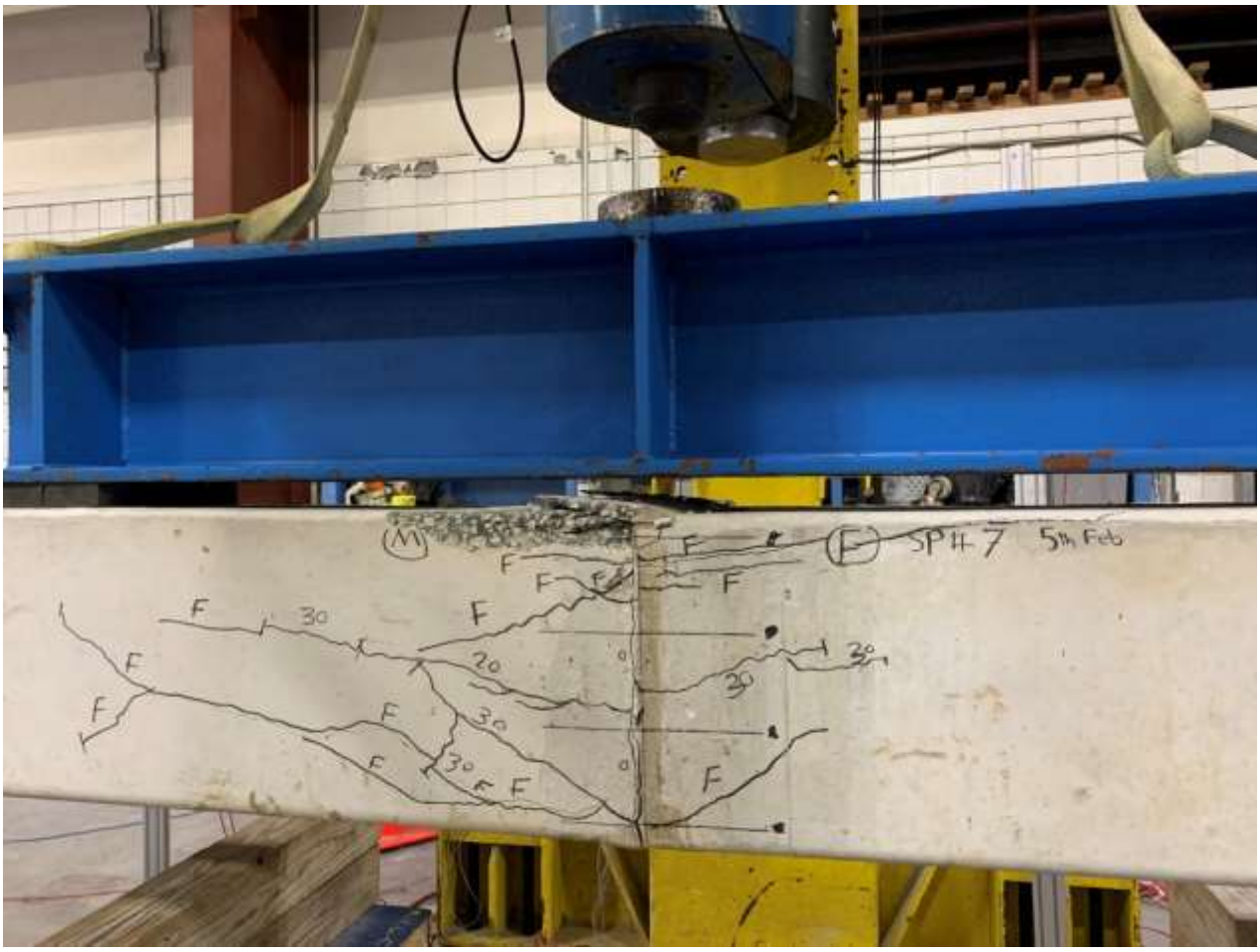

Figure 58: Crack propagation and failure mode of Specimen 7

For Specimen 7, the load-displacement curve, load-deflection profile, crack-opening profile, and load-crack opening curve were plotted, as shown in Figures 59-62, respectively.

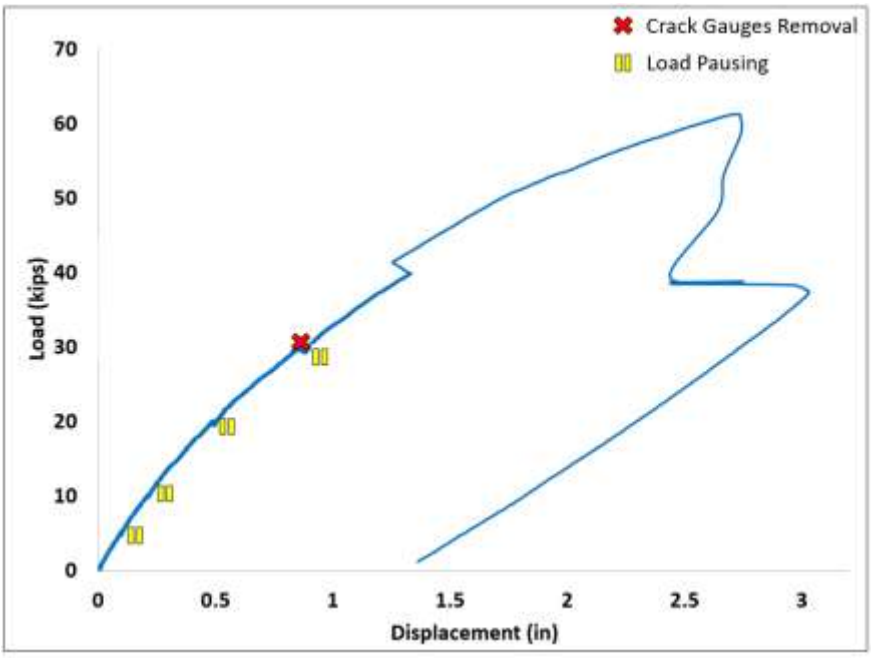

Figure 59: Load-displacement curve for Specimen 7

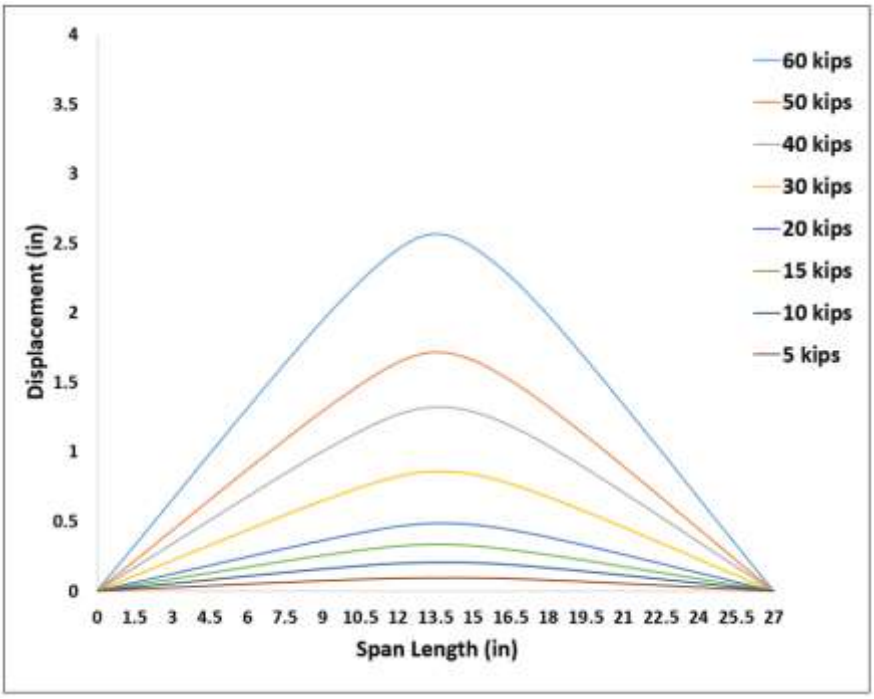

Figure 60: Load-deflection profile for Specimen 7

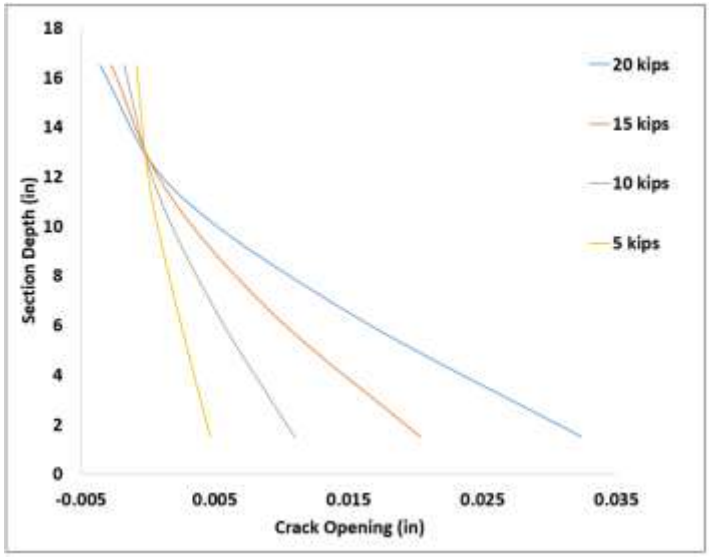

Figure 61: Crack-opening profile for Specimen 7

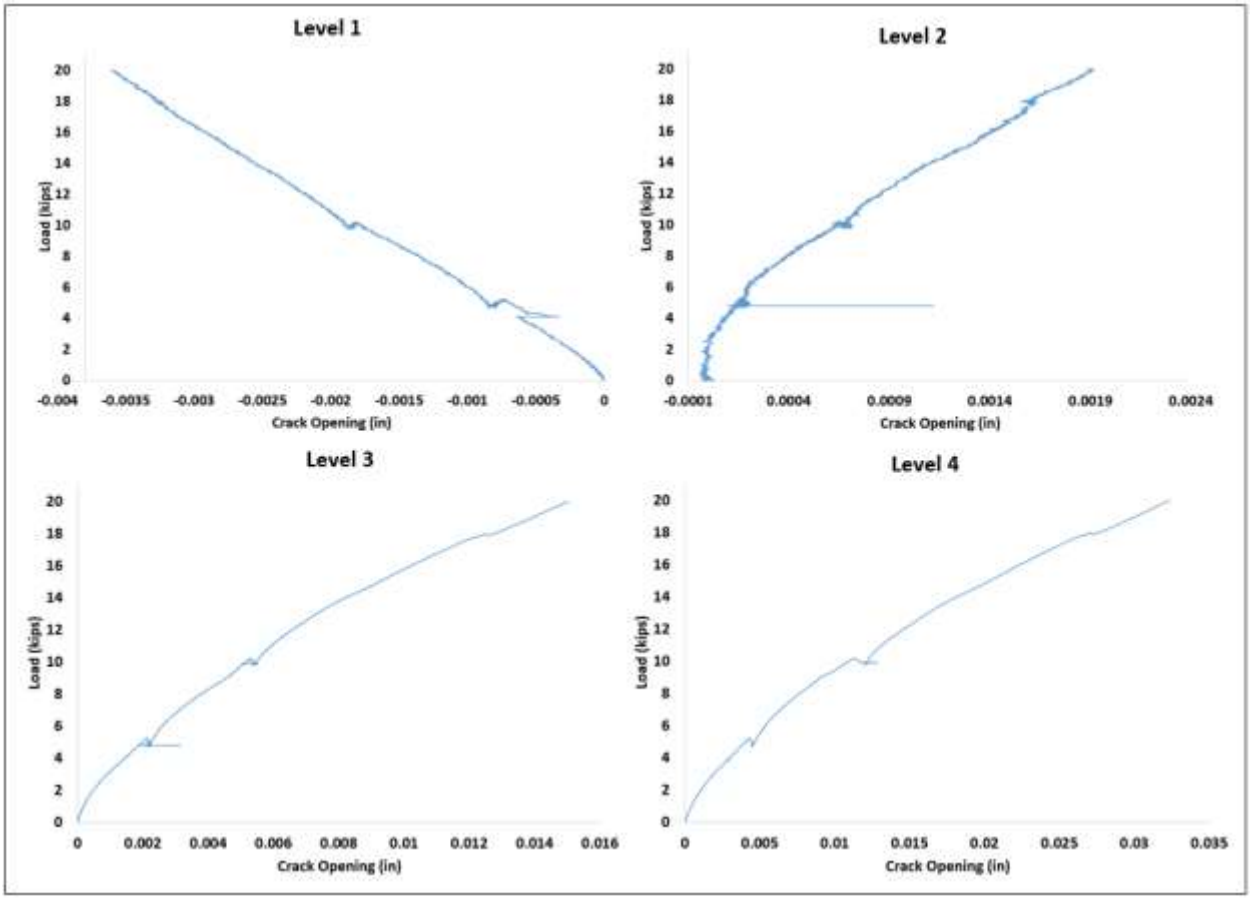

Figure 62: Load-crack opening curves for Specimen 7

5.8 Specimen 8

In Specimen 8, a crack was observed in the splice section prior to the test setup. In this test, the first new flexural crack was observed at splice section at Step 1, load $\leq$ 5 kips. Furthermore, the first splitting crack was detected at Step 2 (load $\leq$10 kips) at the midsection level. As the load increased, additional splitting cracks developed on both sides of the splice section at the level of the lowest strands and midsection. These cracks extended farther until the specimen failed at 59.82 kips with the concrete crushing at the top of the pile near the splice section. Figure 63 shows the failure mode and crack pattern for this test specimen. The maximum moment capacity was calculated for this specimen to be 340.75 k-ft, taking into account the moment from the self-weight of the specimen and the spreader beam.

Figure 63: Crack propagation and failure mode of Specimen 8

For Specimen 8, the load-displacement curve, load-deflection profile, crack-opening profile, and load-crack opening curve were plotted, as shown in Figures 64-67, respectively.

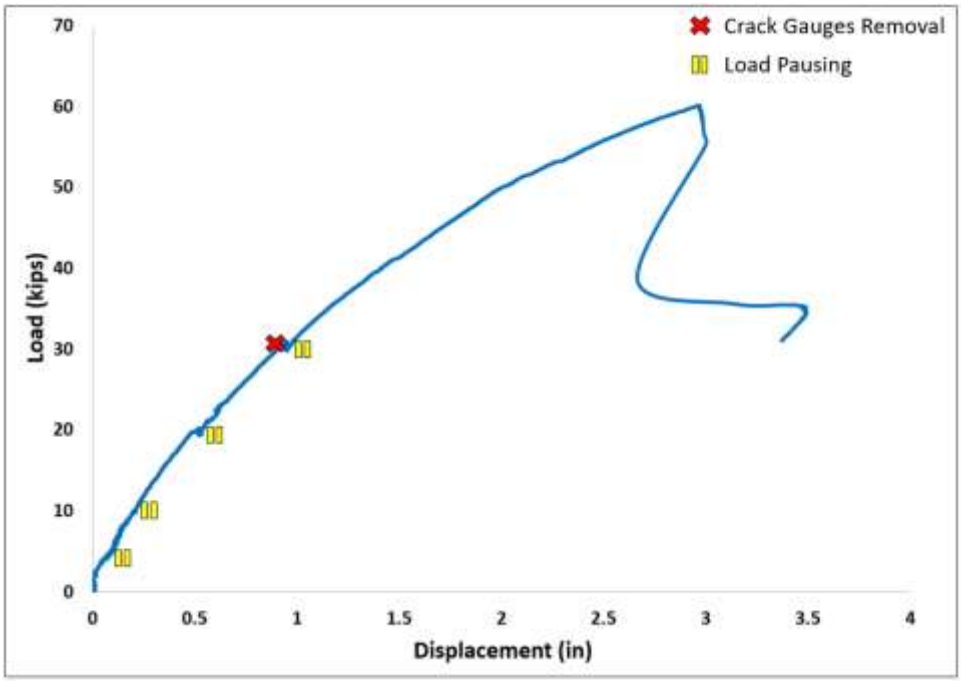

Figure 64: Load-displacement curve for Specimen 8

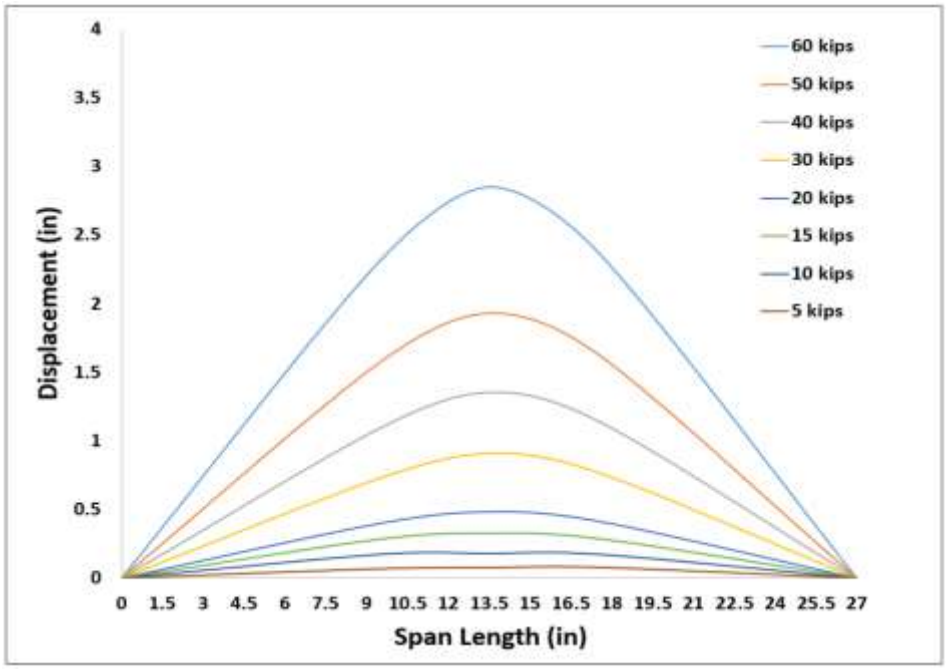

Figure 65: Load-deflection profile for Specimen 8

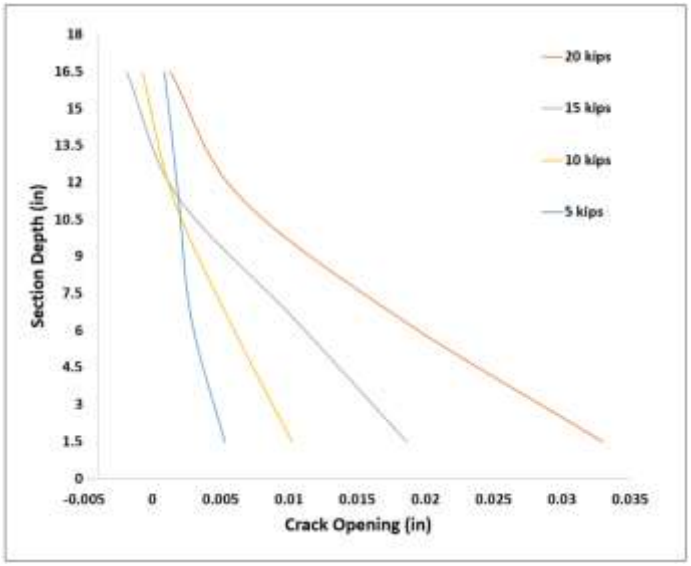

Figure 66: Crack-opening profile for Specimen 8

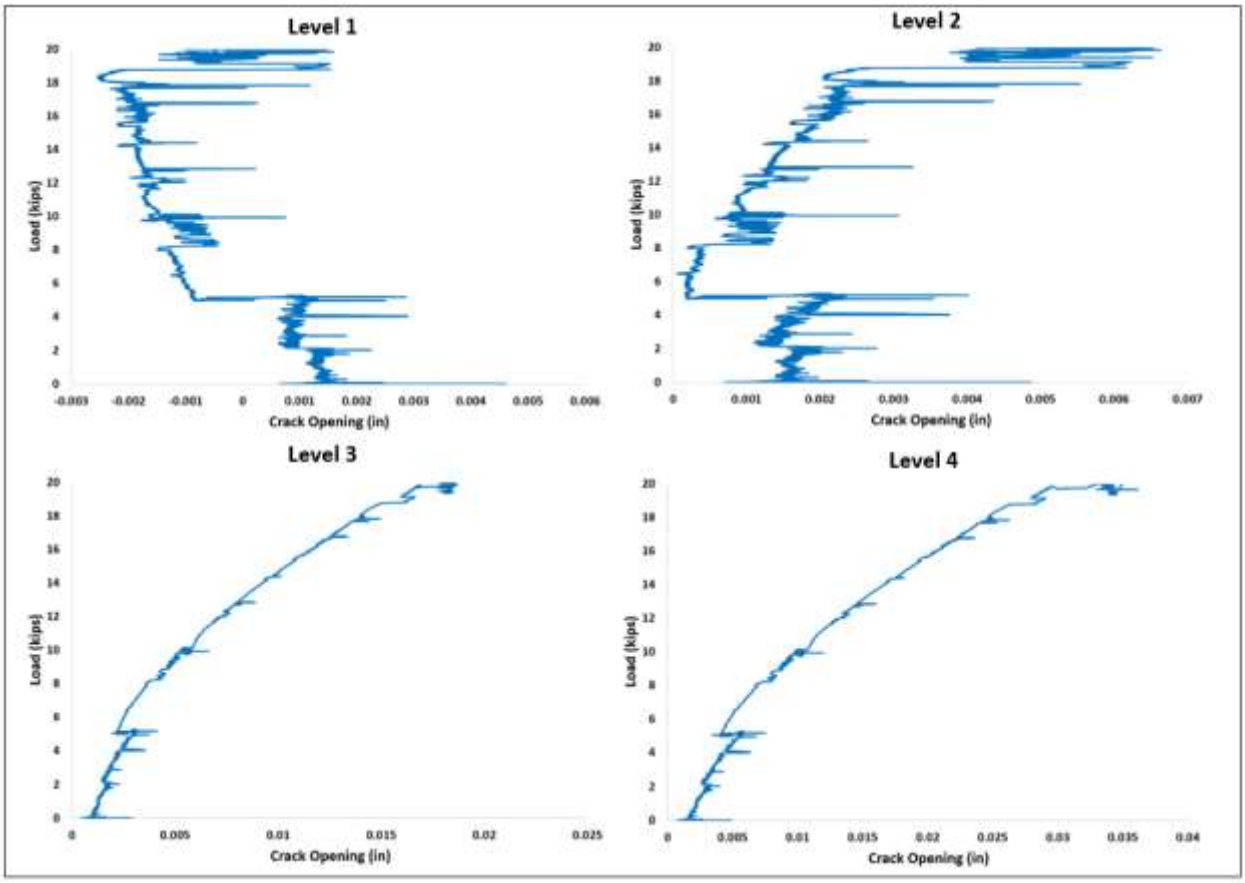

Figure 67: Load-crack opening curves for Specimen 8

5.9 Specimen 9

In Specimen 9, a crack was observed in the splice section prior to the test setup. In this test, the first splitting crack was detected at Step 2 (load ≤10 kips) at the first and second levels of strands from the top of the section. As the load increased, additional splitting cracks developed on both sides of the splice section. These cracks extended farther until the specimen failed at 36.95 kips with the concrete crushing at the top of the pile at the splice section. Figure 68 shows the failure mode and crack pattern for this test specimen. The maximum moment capacity was calculated for this specimen to be 223.54 k-ft, taking into account the moment from the self-weight of the specimen and the spreader beam.

Figure 68: Crack propagation and failure mode of Specimen 9

For Specimen 9, the load-displacement curve, load-deflection profile, crack-opening profile, and load-crack opening curve were plotted, as shown in Figures 69-72, respectively.

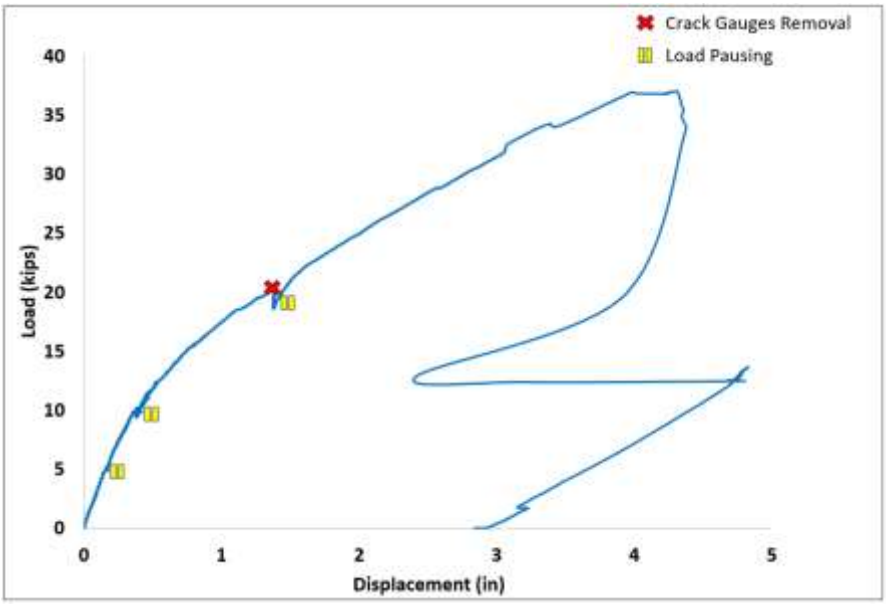

Figure 69: Load-displacement curve for Specimen 9

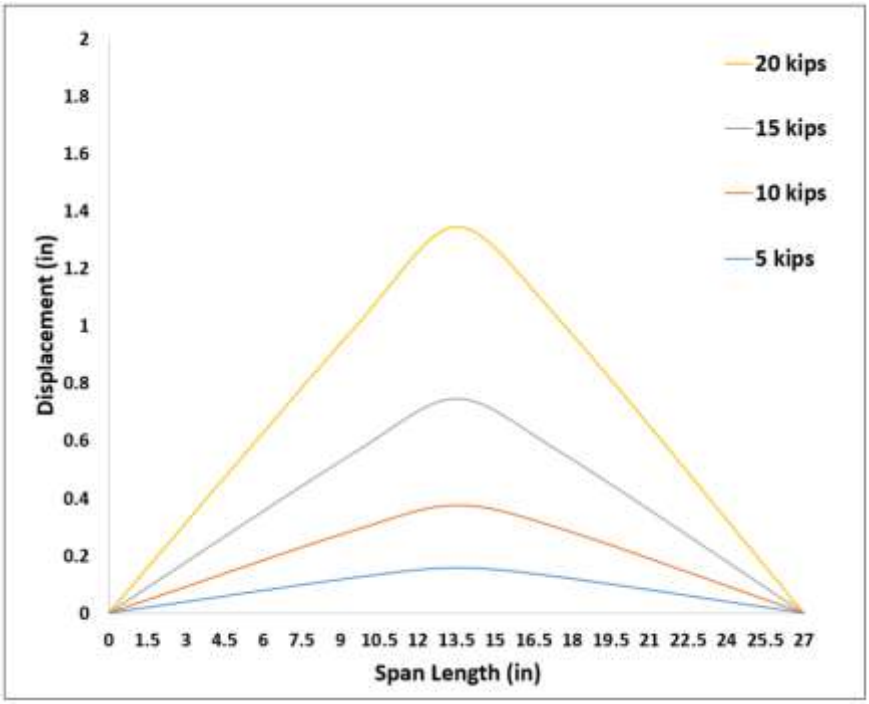

Figure 70: Load-deflection profile for Specimen 9

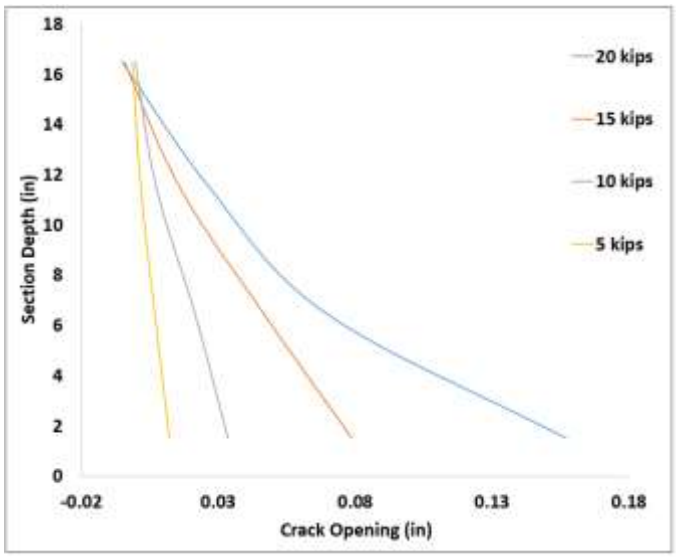

Figure 71: Crack-opening profile for Specimen 9

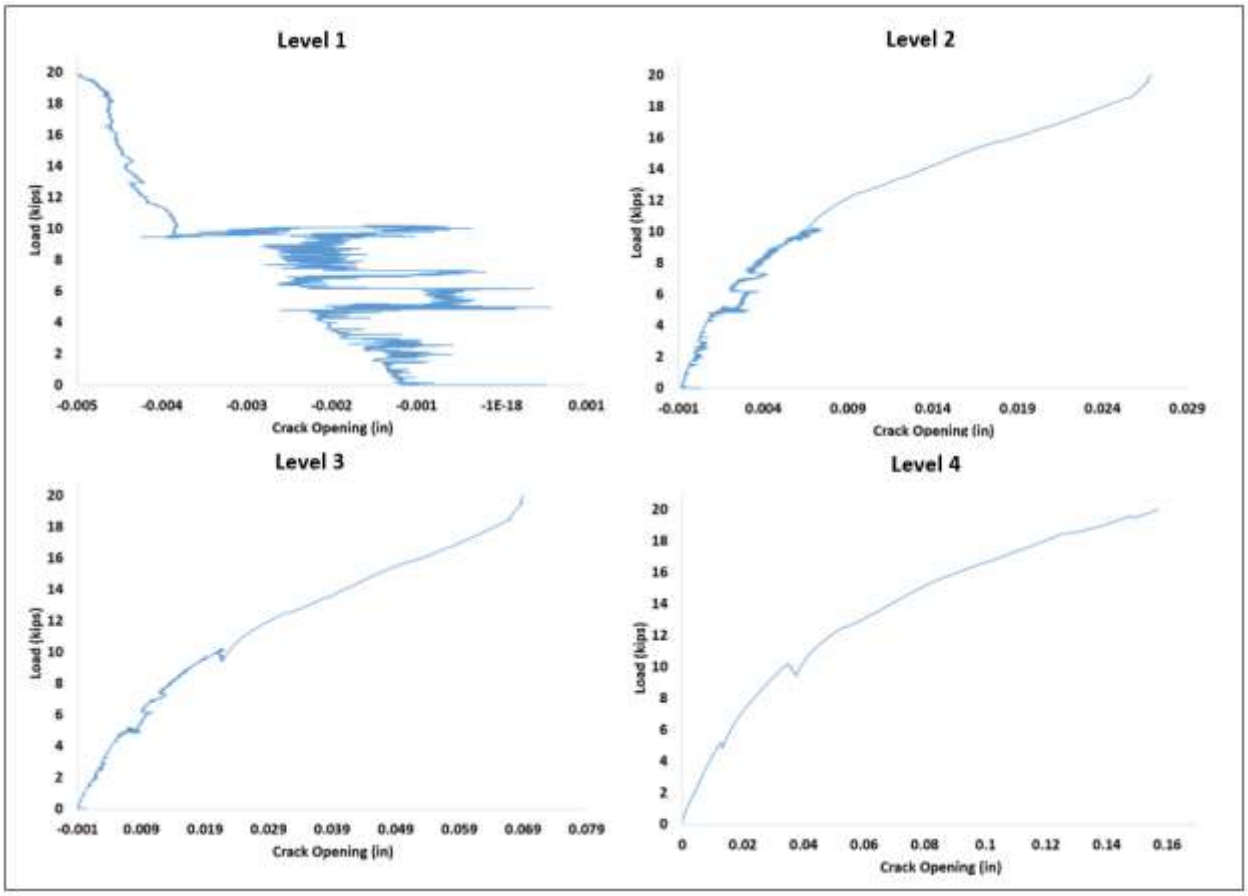

Figure 72: Load-crack opening curves for Specimen 9

5.10 Specimen 10

In Specimen 10, a crack was observed in the splice section prior to the test setup. In this test, the first new flexural crack was observed in the splice section at Step 2 (load ≤10 kips). In addition, the first splitting crack was detected at Step 2 (load ≤10 kips) at the second level of strands from the top and midsection. As the load increased, additional splitting cracks developed on both sides of the splice section. These cracks extended farther until the specimen failed at 40.98 kips with the concrete crushing at the top of the pile at the splice section. Prior to the concrete crushing, horizontal and vertical cracks showed large openings consistent with splitting due to bond failure in the male segment. Figure 73 shows the failure mode and crack pattern this test specimen. The maximum moment capacity was calculated for this specimen to be 244.19 k-ft, taking into account the moment from the self-weight of the specimen and the spreader beam.

Figure 73: Crack propagation and failure mode of Specimen 10

For Specimen 10, the load-displacement curve, load-deflection profile, crack-opening profile, and load-crack opening curve were plotted. as shown in Figures 74-77, respectively.

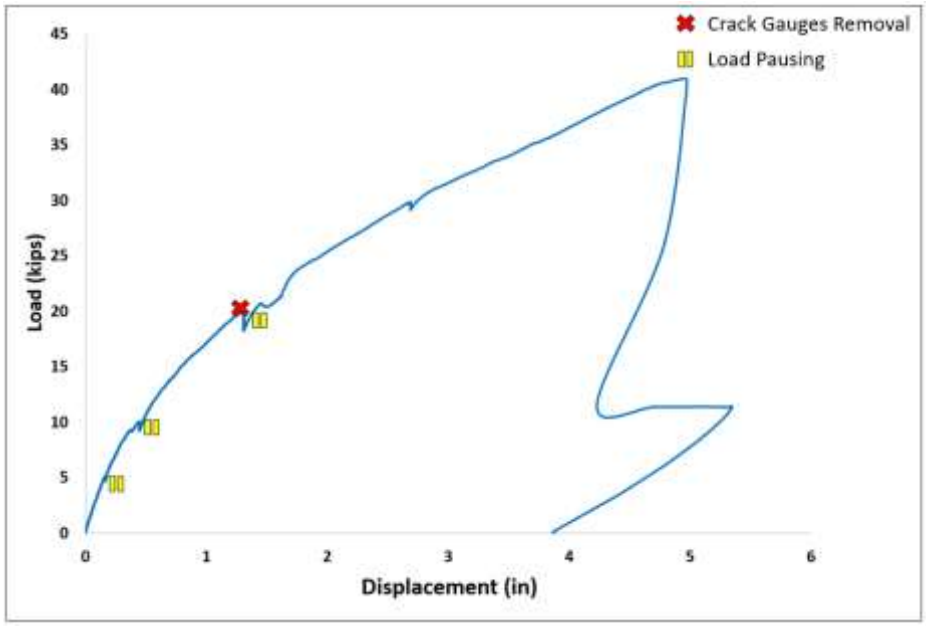

Figure 74: Load-displacement curve for Specimen 10

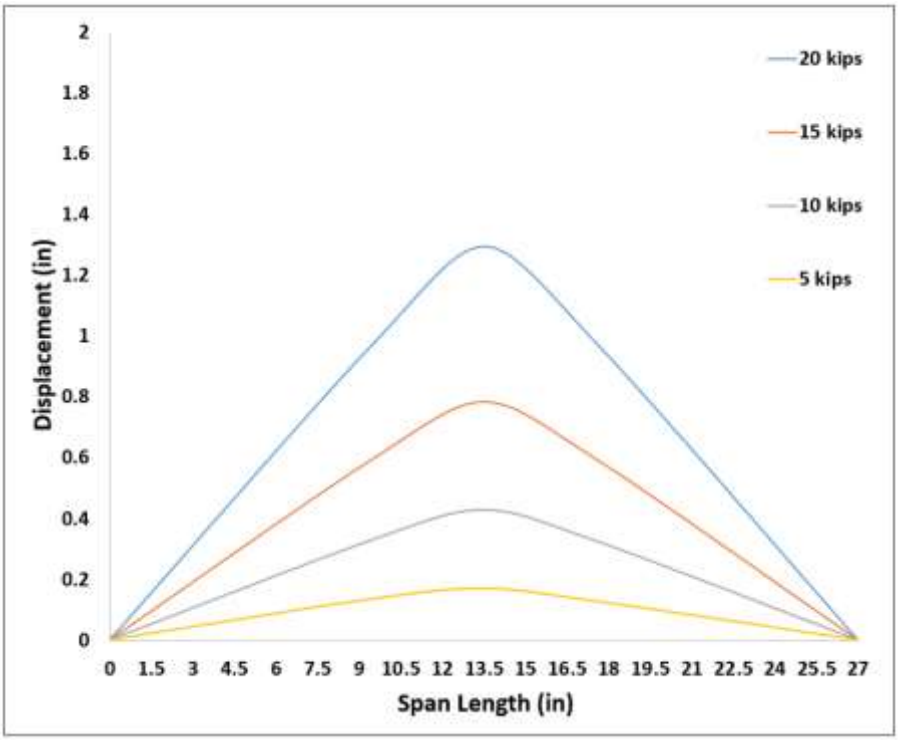

Figure 75: Load-deflection profile for Specimen 10

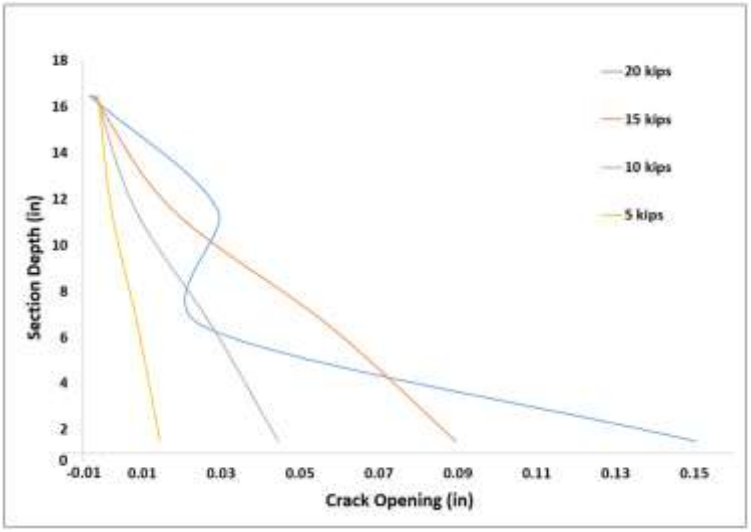

Figure 76: Crack-opening profile for Specimen 10

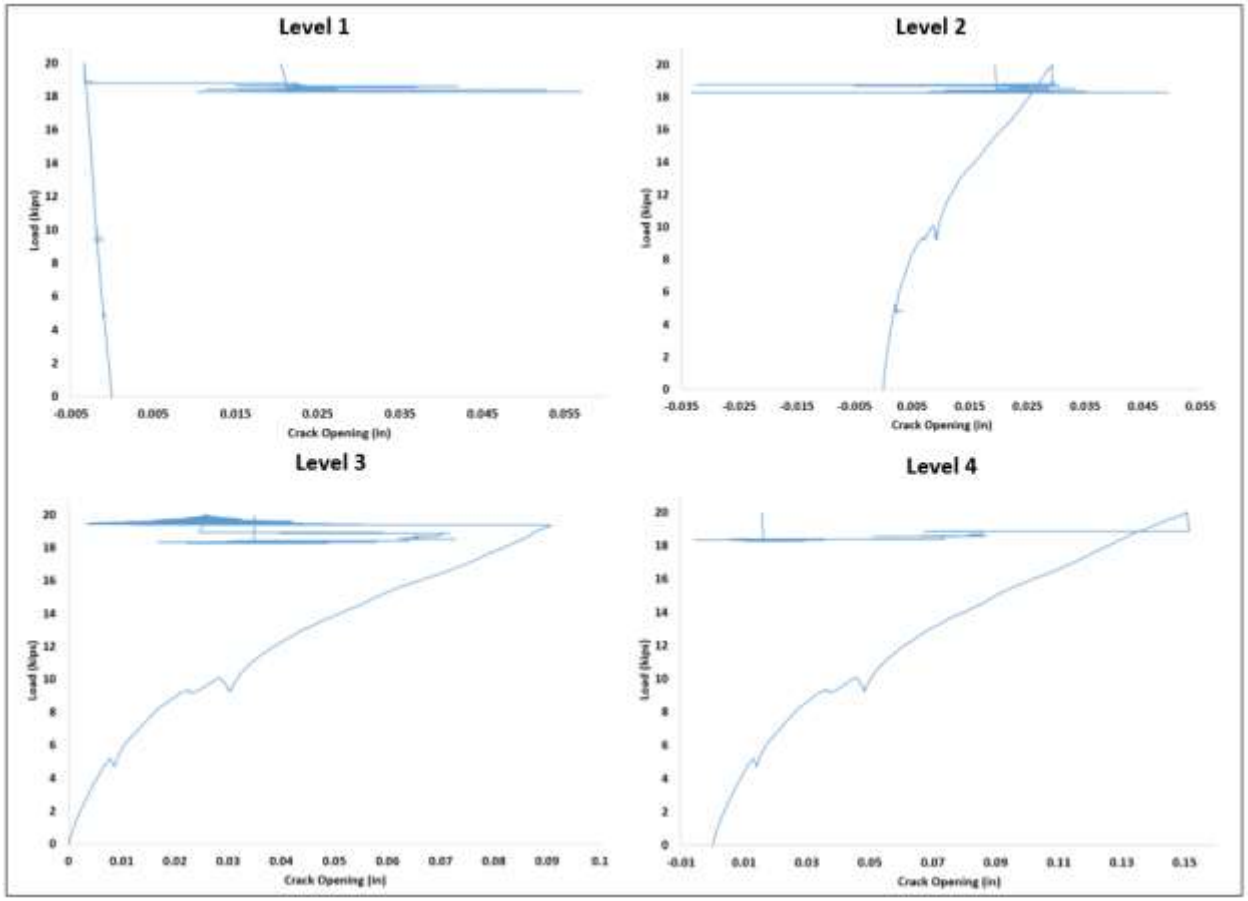

Figure 77: Load-crack opening curves for Specimen 10

5.11 Summary of test results

Table 12 summarizes the test results for all specimens and compares the moment capacity obtained from the test to the estimated nominal moment capacity using the analytical procedure developed in Task 2. With the exception of unforeseen specimens (Specimens 1 and 2), the estimated nominal moment capacities are in very good agreement with the test results. More importantly, the nominal moment capacity estimation is conservative for all preplanned specimens. For the case of unforeseen specimens, it was expected that the test capacities would be lower than estimated because of the shorter than required dowel lengths and missing auxiliary bars,

Table 12: Moment capacity for all test specimens

Specimen Number	Estimated Nominal Moment Capacity		Moment Capacity from Test	Percentage Difference	
	Concrete Strength			Concrete Strength	
	6.5 ksi	7.3 ksi		6.5 ksi	7.3 ksi
1	222.74 k-ft	233.26 k-ft	178.13 k-ft	-20.03	-23.63
2	222.74 k-ft	233.26 k-ft	139.39 k-ft	-37.42	-40.24
3	222.74 k-ft	233.26 k-ft	247.98 k-ft	11.334	6.3127
4	222.74 k-ft	233.26 k-ft	245.63 k-ft	10.275	5.302
5	222.74 k-ft	233.26 k-ft	263.05 k-ft	18.098	12.772
6	222.74 k-ft	233.26 k-ft	257.57 k-ft	15.637	10.421
7	305.1 k-ft	323.4 k-ft	347.67 k-ft	13.952	7.5035
8	305.1 k-ft	323.4 k-ft	340.75 k-ft	11.684	5.3641
9	198.02 k-ft	207.2 k-ft	223.59 k-ft	12.887	7.8855
10	198.02 k-ft	207.2 k-ft	244.19 k-ft	23.317	17.854

5.12 Observation unforeseen specimens

To accommodate drilling of 1-3/4 –in. holes for unforeseen specimens, the precast plant embedded 1-1/2-in. PVC pipes to enlarge later with drilling. They stated that the trajectory was difficult to observe once the head of the bit passed the face of the concrete pile. The 3-ft long drill bit used to perform the holes was warping due to heating and pressure. To correct the warping, they were changing the bit as often as possible to give it time to cool off. Since the holes were performed horizontally, the pressure applied was different from person to person. Also the difference in height of the personnel who performed the holes was substantial, therefore applying pressure upward or downward based on their height. Since the opening of the hole at the splice face had the required size and shape, they were not able to verify the final shape of the hole inside the body of the pile. Consequently, misalignment was introduced for the holes drilled in unforeseen segments. Dissection of unforeseen specimens tested showed no major misalignment for Specimen 1 (see Fig. 27), but indicated noticeable misalignment for Specimen 2 (see Fig. 33). Accordingly, the authors believe that the lower capacity obtained in Specimen 2 is a consequence of applied misalignment affecting the development and progression of splitting cracks and debonding.

5.13 Failure mode observations

Mode of failure is referred to the mechanism developed at or near maximum load and resulting in significant drop in capacity from its maximum. Three modes of failure could be observed for the test specimens; 1- Classical flexural failure with crushing of concrete in the compression zone at splice section, 2- flexural cracking/debonding in the male segment near the end of dowel, and 3- splitting and bond failure for the dowels in the female segment.

1- Classical flexural failure:

For Specimens 3, 4, 7, 8, 9 and 10, the failure mode followed the classical flexural failure mechanism with crushing of concrete. This is an indication that development lengths for dowels and auxiliary bars (if any) were adequate to allow this mode to occur. Figure 43 shows an example of this type of failure mode. Although, splitting cracks were developed and propagated, the confinement seems to have been adequate to keep the dowels engaged until the failure.

2- Flexural cracking/debonding in the male segment:

For Specimens 5 and 6, the failure mechanism was initiated by flexural cracking and concrete spalling in the male segment at the section near the end of the dowel bar. The load resistance dropped significantly with this cracking indicating potential debonding of strands at the cracked section which can also be attributed to lack of adequate confinement at this location (closely-spaced spirals were implemented only in the female segments for the first 4 ft from the splice section). Figure 48 shows an example of this type of failure mode. Concrete crushing shown in the figure above the cracked section occurred after continuing the test beyond maximum at much lower loads. Apparently Specimens 9 and 10 with identical dowel length but CFRP dowels instead of GFRP did not failed similarly, likely for the fact that the splice section with CFRP failed earlier with classical flexural mode.

3- Splitting and bond failure in the female segment:

For unforeseen test specimens, Specimens 1 and 2, the failure occurred with splitting of concrete cover, bond failure of dowels in female segment, and horizontal and vertical crack opening at the section near the end of dowel. Figure 32 shows an example of this type of failure mode.

Splitting crack from bond action were observed for all tested specimens. Figure 78, shows cross section of a dissected specimen after the test. Splitting cracks are visible mostly at the level of strands. In some cases, as the example in this figure, enlargement of the splitting cracks likely because of inadequate confinement, resulted in debonding of the strands or dowels.

Figure 78: Dissection of Specimen 5

The analysis and interpretation of the test results will be included in the next deliverable for Task 5.

6 REFERENCES

Standard Plans – Index Series 455. Florida Department of Transportation, Tallahassee, 2020-2021.

Standard Specifications for Road and Bridge Construction. Florida Department of Transportation, Tallahassee, January, 2020.